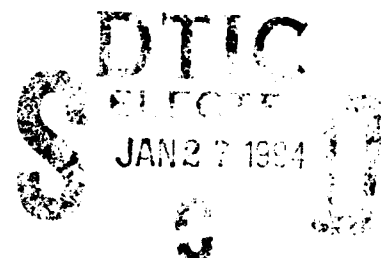# NAVAL POSTGRADUATE SCHOOL
MONTEREY, CALIFORNIA

AD-A275 169

DTIC

JAN 2 7 1994

THESIS

The Quantitative Microstructural Characterization of Multipass TIG Ultra Low Carbon Bainitic Steel Weldments and Correlation with Mechanical Properties.

by

Daniel E. Butler

September 1993

Thesis Advisor: Alan G. Fox

Approved for public release; distribution is unlimited.

94-02738

94 1 26 188

REPORT DOCUMENTATION PAGE

1. AGENCY USE ONLY (Leave blank)	2. REPORT DATE 1993, September	3. REPORT TYPE AND DATES COVERED From: 04/93 To: 09/93

4. TITLE AND SUBTITLE
The Quantitative Microstructural Characterization of Multipass TIG Ultra Low Carbon Bainitic steel Weldments and correlation with Mechanical Properties.

5. FUNDING NUMBERS

6. AUTHOR(S)

Daniel E. Butler

7. PERFORMING ORGANIZATION NAME(S) AND ADDRESS(ES)

Mechanical Engineering Department
Naval Postgraduate School
Monterey CA 93943-5000

8. PERFORMING ORGANIZATION REPORT NUMBER

9. SPONSORING/MONITORING AGENCY NAME(S) AND ADDRESS(ES)

David Taylor Research Center
Annapolis MD 21402

10. SPONSORING/MONITORING AGENCY REPORT NUMBER

11. SUPPLEMENTARY NOTES

The views expressed in this thesis are those of the author and do not reflect the the official policy or position of the Department of Defense or the United States Government.

12a. DISTRIBUTION/AVAILABILITY STATEMENT

Approved for public release: Distribution Unlimited

12b. DISTRIBUTION CODE

A

13. ABSTRACT (Maximum 200 words)

The U.S. Navy has maintained a continuous research, development and certification program in ULCB steels as a possible replacement for the HY and HSLA steels currently being used in ship construction. The overall aim of this program is to develop a high strength steel with improved weldability. Improved weldability could eliminate the requirement of preheating, (a necessary and costly step required to prevent weld metal cracking in HY steels). The strength of ULCB steel weldments can be correlated to the weld metals composition in a simple manner, however the toughness of the weldment seems to fluctuate in complex manner depending on the weld metal composition, weld power, and possibly the non-metallic inclusion size, type, number and distribution. This study attempted to correlate the embrittlement of ULCB/ULCB multipass TIG weldments to the given microstructure and to the type, size, number and distribution of the nonmetallic inclusions within the weldment. This work led to the following conclusions: (A) The embrittlement of ULCB weldments appeared to be the result of microscopic transgranular cracking. (B) There exists a need to design a process which can manufacture reproducible multipass weldments to facilitate testing, and (C) the type, size, number and distribution of the nonmetallic inclusions did not appear to be a factor in the toughness of the weldments investigated.

14. SUBJECT TERMS

Ultra Low Carbon Bainitc Steel

15. NUMBER OF PAGES
98

16. PRICE CODE

17. SECURITY CLASSIFICATION OF REPORT UNCLASSIFIED	18. SECURITY CLASSIFICATION OF THIS PAGE UNCLASSIFIED	19. SECURITY CLASSIFICATION OF ABSTRACT UNCLASSIFIED	20. LIMITATION OF ABSTRACT

The Quantitative Microstructural Characterization of Multipass TIG Ultra Low Carbon Bainitic Steel Weldments and Correlation with Mechanical Properties

by
Daniel E. Butler
Lieutenant, United States Navy
B.S., Virginia Military Institute, 1986

Submitted in partial fulfillment of the
requirements for the degree of

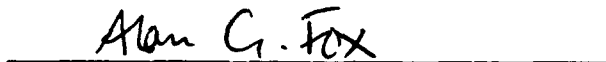## MASTER OF SCIENCE IN MECHANICAL ENGINEERING

from the

NAVAL POSTGRADUATE SCHOOL
September, 1993

Author: _____
Daniel E. Butler

Approved By: _____
Alan G. Fox, Thesis Advisor

_____
Matthew D. Kelleher, Chairman,
Department of Mechanical Engineering

ii

ABSTRACT

The U.S. Navy has maintained a continuous research, development and certification program in ULCB steels as a possible replacement for the HY and HSLA steels currently being used in ship construction. The overall aim of this program is to develop a high strength steel with improved weldability. Improved weldability could eliminate the requirement of preheating, (a necessary and costly step required to prevent weld metal cracking in HY steels). The strength of ULCB steel weldments can be correlated to the weld metals composition in a simple manner, however the toughness of the weldment seems to fluctuate in complex manner depending on the weld metal composition, weld power, and possibly the non-metallic inclusion size, type, number and distribution. This study attempted to correlate the embrittlement of ULCB/ULCB multipass TIG weldments to the given microstructure and to the type, size, number and distribution of the nonmetallic inclusions within the weldment. This work led to the following conclusions; (A) The embrittlement of ULCB weldments appeared to be the result of microscopic transgranular cracking, (B) There exists a need to design a process which can manufacture reproducible multipass weldments to facilitate testing, and (C) the type, size, number and distribution of the nonmetallic inclusions did not appear to be a factor in the toughness of the weldments investigated.

DTIC QUALITY INSPECTED 5

iii

TABLE OF CONTENTS

LIST OF FIGURES

LIST OF TABLES

ACKNOWLEDGEMENTS

I. INTRODUCTION

Ultra Low Carbon Bainitic (ULCB) steels are a relatively new class of steel. ULCB steels gain substantial strength partially through complex alloying and are found to be easily welded due to their "Ultra Low Carbon" weight percentages (< 0.02 Wt %). The complex nature of the alloy interactions is not yet fully understood and thus further investigation is required to optimize the mechanical properties of ULCB steels while minimizing manufacturing cost.

The U.S. Navy has maintained a continuous research, development and certification program in ULCB steels as a possible replacement for the HY and HSLA steels, which are currently being used in ship construction. The overall aim of this program is to develop steels with improved weldability and high strengths. The improved weldability of ULCB steels allows welding processes to take place without the substantial preheating (and/or other stringent welding controls) required when welding HY steels. Preheating is a necessary and costly step required to prevent weld metal cracking in HY steels.

The strength of ULCB steel weldments can be correlated to the weld metal composition in a simple manner, however the toughness of the weldment seems to fluctuate in complex manner depending on the weld metal composition, microstructure, weld power and possibly the non-metallic inclusion size, type, number and distribution, (McDonald, 1992).

This study attempts to correlate the embrittlement of ULCB/ULCB multipass TIG weldments to the microstructure and to the type, size, number, and distribution of the non-metallic inclusions within the weldments.

1

II. BACKGROUND

A. CHARACTERISTICS OF HY AND HSLA STEEL

High Yield (HY) steels derive their strength through conventional quench and temper techniques. Carbon and other alloys such as Cr, Mn, Ni, and Mo are added for strengthening, improving hardenability, and other effects. The high carbon content (0.6 to 1.4 Wt% C) of HY steels place severe restrictions on the cooling rates that must be maintained during the processing and welding of these steels. A fast cooling rate is required to obtain the desired strength, however if the cooling rate is excessive, the formation of a martensitic microstructure will result. A martensitic microstructure is very brittle and extremely susceptible to Hydrogen Induced Cracking (HIC). To avoid this problem it is necessary to conduct extensive preheating of the HY steel prior to welding, and a stringent control of the weld heat input and interpass temperature must be maintained at all times during the welding process. This makes the welding of HY steels very difficult and costly.

High Strength Low Alloy (HSLA) steels were developed over the past decade with the intent of replacing HY steels for Naval applications. HSLA steels are low carbon (0.05 Wt% C), precipitation strengthened, solid solution strengthened steels which receive a final non-recrystallization thermomechanical roll pass to obtain the desired strength. The reduced carbon content of HSLA steel allows the welding process to be carried out without the extensive preheating requirements of HY steel. This equates to a significant savings in time and expense for major construction projects.

2

The U.S. Navy currently demands steels with significantly higher strengths and improved weldability (ability to resist HIC) in order to produce ships and submarines that are lighter, stronger, and less costly to fabricate. The Graville diagram, see Figure 2.1, illustrates that a steel of this nature will require an extremely low carbon content (for improved weldability) and yet a high carbon equivalent (for the required high strength and hardenability). Review of the Graville diagram shows that ULCB steels meet these requirements. The placement of HY and HSLA steels on the Graville diagram should also be noted.
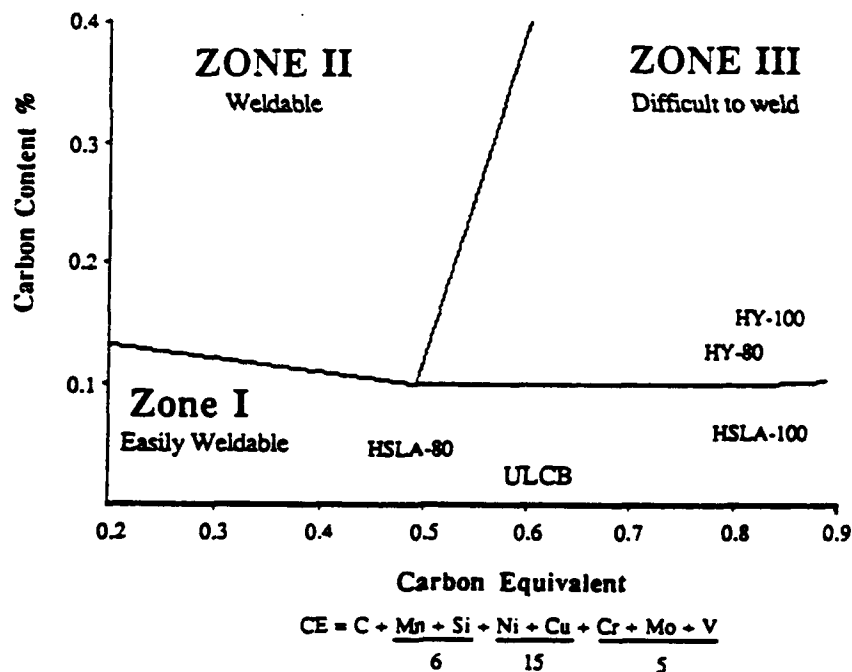
Figure 2.1   Graville Diagram
(Blicharski et al, 1989, p.318)

B. CHARACTERISTICS OF ULCB STEEL

Ultra Low Carbon Bainitic (ULCB) steels are currently being developed as a possible alternative to HY and HSLA steels. The extremely low carbon content of ULCB steels (< 0.02 Wt%C) allows these steels to be designed with yield strengths greater than 690MPa (100Kpsi) and yet be easily welded. The weldability of ULCB steels is shown graphically in Figure 2.1 and can also be derived from Figure 2.2. Figure 2.2 shows that ULCB steels are almost cooling rate insensitive, (ie; the strength is not greatly increased with increased cooling rates thus brittle microstructures are not readily being formed). ULCB steels derive their strengths through solid solution strengthening and advanced non-recrystallization thermomechanical processing. The Naval Surface Warfare Center, Annapolis Detachment has recently shown that the strength of ULCB weldments can be accurately predicted, see Figure 2.3. However, the toughness of these weldments seems to fluctuate in a complex manner depending on the weld metal composition, weld power, and possibly the presence of non-metallic inclusions, (McDonald, 1992).

Through alloy management, bainitic microstructures are predominantly formed during the weldment of ULCB steels. Bainite consist of fine cementite (Fe_3C) particles surrounded by a ferrite matrix. This microstructure exhibits a desirable combination of strength and toughness, (Callister, 1985, p.325). The formation of bainite is through a partial shear transformation from austenite, (partial shear transformations being nearly spontaneous with little diffusion required). Bainite often forms in conjunction with martensite, acicular

4
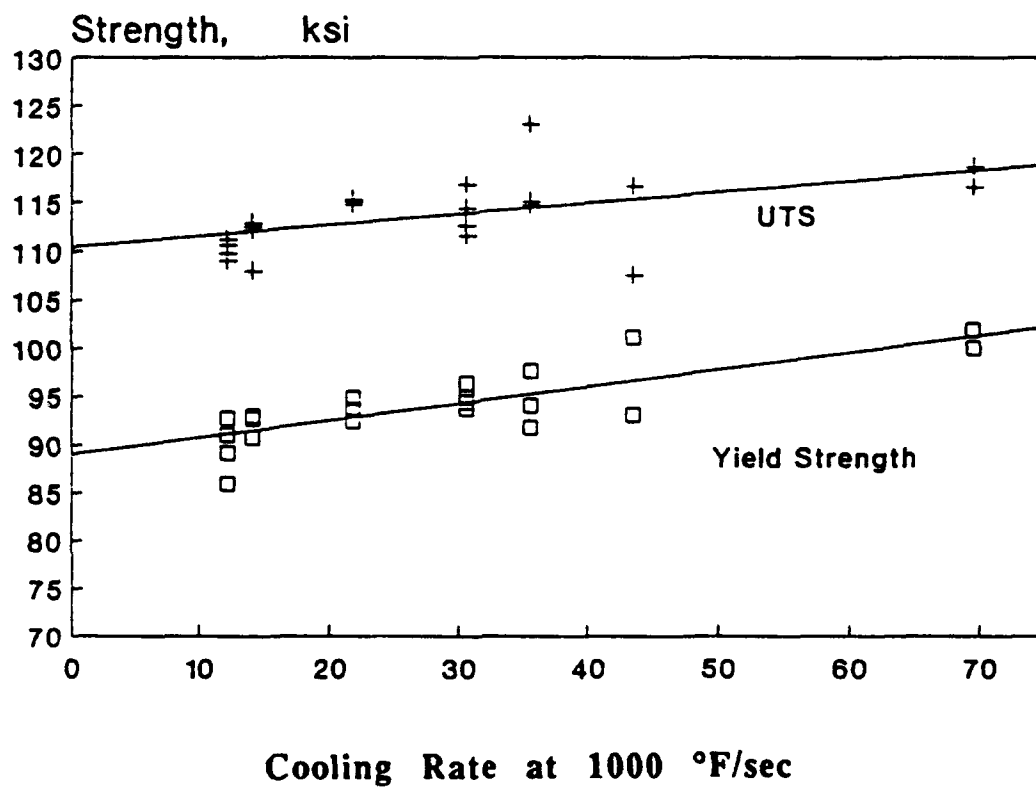
Figure 2.2   **Measured Strength for ULCB 8033**
(NSWC, 1993, p.30)
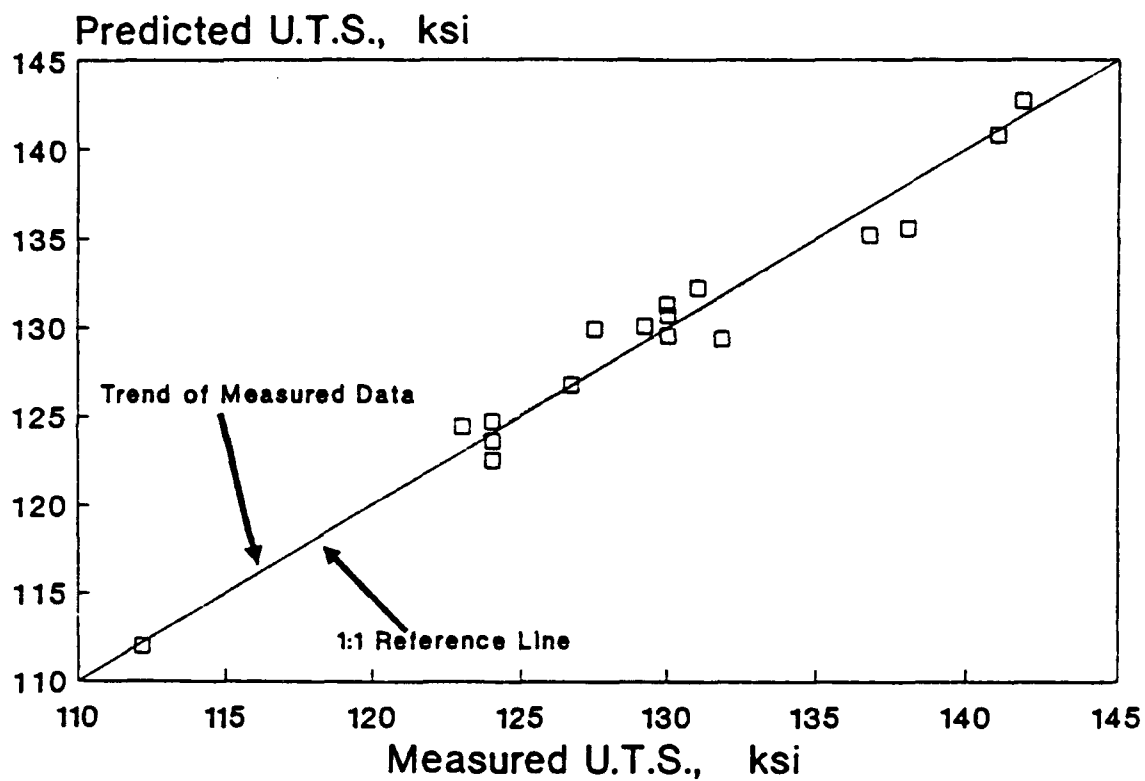
Figure 2.3 Measured vs Predicted UTS for ULCB Welds (NSWC, 1993, p.51)

ferrite, Widmanstatten ferrite, retained austenite, or pearlite and is therefore often difficult to properly identify. Of these other microstructures, acicular ferrite is the most desired. The microstructure of acicular ferrite is interlocking and can improve the toughness of weldments. Large numbers of inclusions are required to nucleate acicular ferrite, thus for reasons discused in future sections, acicular ferrite is not expected in TIG weldments.

The alloying elements used in ULCB steels are; Carbon (C), Manganese (Mn), Molybdenum (Mo), Nickel (Ni), Niobium (Nb), Chromium (Cr), Aluminum (Al), Silicon (Si), and Titanium (Ti). The majority of these elements, (C, Ni, Cr, Mo, and Mn), are used to increase hardenability; Nb is used to help control grain size; and Al, Si, and Ti are primarily used as deoxidizing agents. With an ultra low carbon content, ULCB steels rely heavily on the combined strengthening effects of the other mentioned alloying elements. These "other" alloys are required in relatively large concentrations (approximately 10 Wt% combined), and being more costly than carbon add to the expense of ULCB steel production. To minimize the production cost and optimize the mechanical properties a firm understanding must be obtained into the complex nature in which these alloys inter-react during the welding process.

C. WELDING PROCESSES

1. Tungsten Inert Gas (TIG) Welding

Tungsten Inert Gas (TIG) Welding (or Gas Tungsten Arc Welding (GTAW)), produces welds of outstanding quality. In TIG welding a nonconsumable tungsten electrode is used to maintain an electric arc to the work-piece, thus heat is generated and the work-piece locally melted. The molten weld pool is shielded from the atmosphere with an inert gas, usually argon or helium. Figure 2.4 provides a sketch of the TIG welding process. TIG welding has the following advantages: (A) The nonconsumable electrode produces a very stable arc; (B) Direct Current Straight Polarity ((DCSP) - electrode negative) can be utilized, thus directing 2/3 of the generated heat at the weldment producing deep welds with shallow HAZs; (C) The filler wire can be fed directly into the weld pool thus reducing the chance of alloy vaporization and oxidation; and (D) the filler wire shape is relatively insignificant thus greatly simplifying the process required to obtaining experimental filler wires; (Stinchcomb, 1989, p.123-129). The above attributes make TIG welding a very "clean" welding process, ideal for industrial applications as well as for research.

2. Metal Inert Gas (MIG) Welding

In Metal Inert Gas (MIG) Welding (or Gas Metal Arc Welding (GMAW)), see Figure 2.5, a consumable electrode is used to maintain an electric arc to the base metal, thus allowing the melting of the base metal and the deposition of the filler material to be accomplished in one step. The above improves the speed and compactness of MIG welding over TIG welding, but at the expense of producing a weld of slightly poorer quality. The reduction in

8
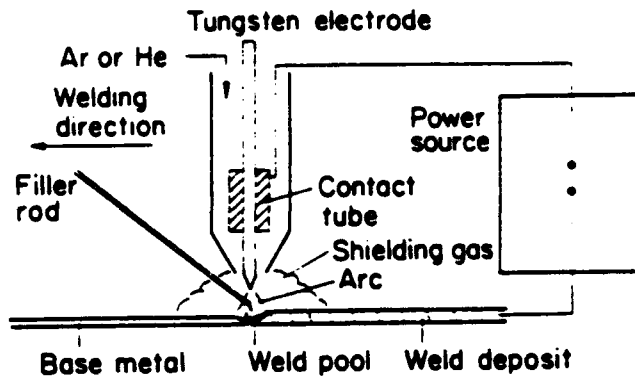
Figure 2.4   Tungsten Inert Gas (TIG) Welding Process
(Kou, 1987, p.10)
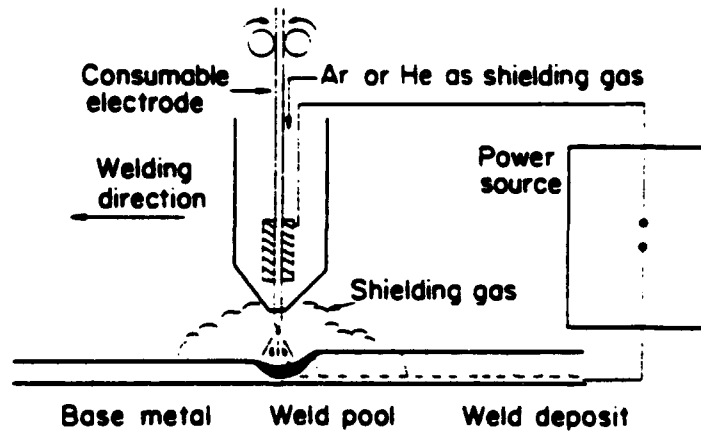
Figure 2.5   Metal Inert Gas (MIG) Welding Process
(Kou, 1987, p.16)

9

the MIG weld quality can be attributed to the following: (A)The consumable electrode produces an unstable arc which can adversely effect the ability of the shield gas to protect the weld pool from atmospheric oxygen and nitrogen; (B) CO_2 is commonly added to the inert shield gas to help stabilize the arc, thus increasing the amount of available oxygen in the weld atmosphere; (C) the filler wire material is "sprayed" at the weld pool, thus the alloys in the filler wire have a greater chance of being vaporized or oxidized; and (D) Direct Current Reverse Polarity {(DCRP) - electrode positive} is often utilized to promote the melting of the consumable "filler wire" electrode. This directs only 1/3 of the generated heat at the weldment and thus shallow welds with relatively large HAZs are produced; (Stinchcomb, 1989, p.188-199). The net result of the above are weldments with increased oxygen and nitrogen contents (see Figure 2.6) and microstructures which are more conducive to mechanical failure. These topics shall be discused in greater detail in the following sections.

It should be noted that the MIG weldment properties discussed above were based on a relative comparison to the TIG welding process only. When the MIG welding process is compared to all of the welding process commercially available, the MIG welding process produces weldments of very high quality.
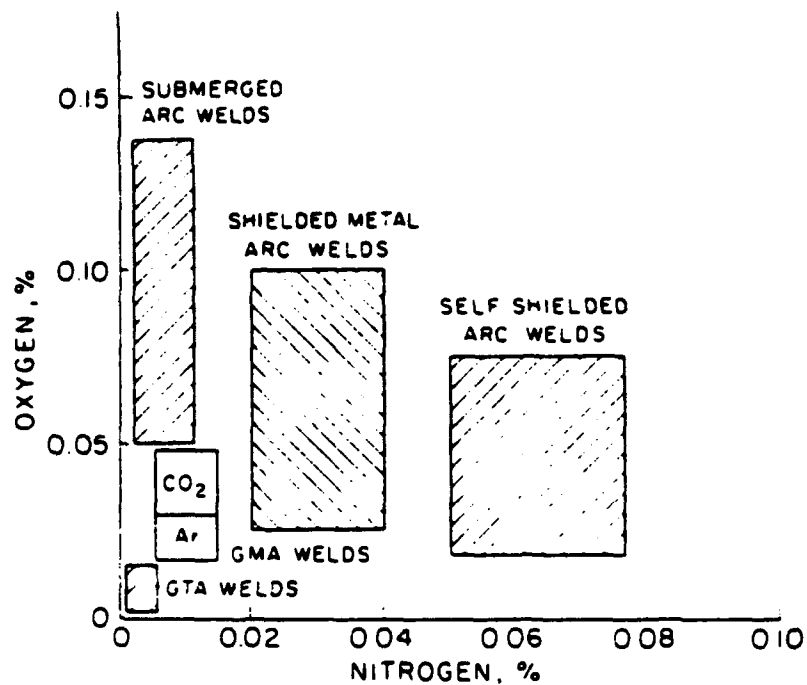
Figure 2.6   Expected Levels Of Oxygen and Nitrogen
in Various Arc Welding Processes
(Kou, 1987, p.63)

11

D. METALLURGICAL PROPERTIES OF WELDMENTS

1. Fusion Zone, Heat Affected Zone, and Base Metal

The microstructure of most carbon steel weldments can be defined by three zones; the Fusion Zone (FZ), the Heat Affected Zone (HAZ), and the Base Metal. The HAZ can further broken to; the Grain Coarsening (GC) region, the Grain Refining (GR) region, and the Partial Grain Refining (PGR) region. The above Zones and Regions are presented schematically for a theoretical single-pass weldment and a theoretical multipass weldment in Figure 2.7 and Figure 2.8 respectively. The development of the microstructures within these regions and zones and their corresponding effects on the strength and toughness of the weldment are discussed below:

The Fusion Zone (FZ) is created by the solidification of the weld metal. The microstructure consists of coarse columnar grains which are relatively weak and lacking in toughness. The size of the columnar grains can be reduced by increasing the weld heat input, the addition of nucleating agents (or inoculates), weld pool stirring, and stimulated surface nucleation, (Kou, 1987, p.154).

The Base Metal is the "Zone" of the weldment in which the microstructure of the original work-piece is represented (ie; the original microstructure of the work-piece is unaltered by the welding process).

12

Fusion Zone (Columnar Grains)   HAZ (Partial Grain Refining)

HAZ (Grain Coarsening)   BASE METAL
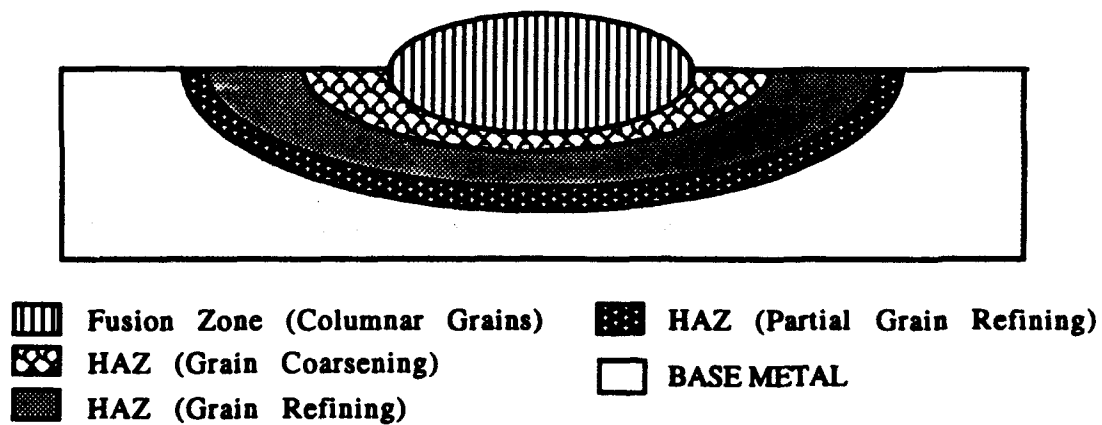
HAZ (Grain Refining)

Figure 2.7   Single-pass Weld Grain Diagram for Steel
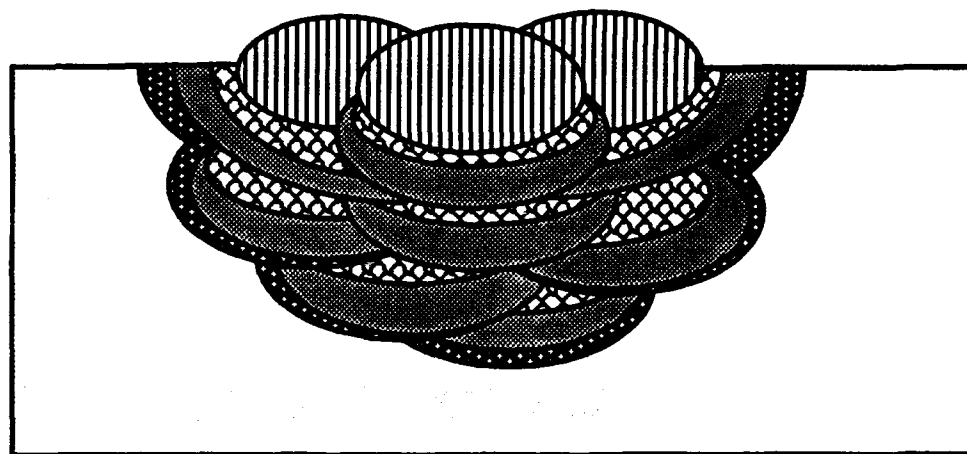
NOTE: Uses Same Grain Key as Figure 2.7

Figure 2.8   Multipass Grain Refinement in Steels

13

The HAZ Partial Grain Refining region is created when the welding process produces a peak temperature which is high enough to re-austenitize a portion of the original grains but not high enough to nucleate new austenite grains. This corresponds to a temperature between the effective lower and effective upper critical temperatures, Ac1 and Ac3, for mild steels. Upon cooling, this region produces a microstructure which is slightly stronger and tougher than the base metal.

In the HAZ Grain Refining (GR) region a sufficient temperature is reached to allow the nucleation of new austenite grains, however the duration of time at this elevated temperature is limited and thus the austenite grains do not have a chance to coarsen. For mild steels this peak temperature is just above the effective upper critical temperature Ac3. Upon cooling this region produces the smallest, strongest, and toughest microstructures within the weldment.

In the HAZ Grain Coarsening (GC) region the temperature obtained is high enough and remains so for a sufficient enough duration to allow the nucleation of new austenite grains and to allow these grains to coarsen. This temperature is well above Ac3 for mild steels. Upon cooling, the GC microstructure consist of larger and less tough grains than those in the GR region, however the GC grains are significantly smaller and tougher than the columnar grains of the fusion zone.

The advantage of a multipass weldment can now be explained. If a multipass weldment is designed and manufactured properly, the weak columnar grains of initial weld passes will be replaced ("grain-refined" or recrystallized) by the HAZs of the subsequent weld passes, (Kou, 1987, p.326). Ideally the weld metal of a multipass weldment should consist entirely of very tough and strong grain refined regions.

2. Influence of Inclusions

Inclusions can be a significant factor in the strength and toughness of a weldment. The size, composition, and population density of the inclusions present will determine if the "significant factor" is beneficial or detrimental to the mechanical properties. Inclusions are normally classified as being exogenous or indigenous. Exogenous inclusions result from the entrapment of slag, firebrick and other refractories, etc. These inclusions are typically large, brittle, sporadic in occurrence, irregular in shape, and almost always detrimental to the weldments mechanical properties. Indigenous inclusions result from weld metal - arc atmosphere interactions and filler metal - base metal interactions. Indigenous inclusions are typically oxides, sulfides, nitrides, or carbides, and can be ether beneficial or detrimental to the weldment. Small inclusions (< 1.0 microns) may be used to improve the strength and toughness of the weld metal and base metal by restricting grain growth and aiding in the nucleation of smaller and more desirable

microstructures, (Kiessling, 1989, p.102). Conversely, large inclusions (> 2.0 microns), can adversely affect the weldments mechanical properties by acting as crack or micro-void initiation sites. Thus small, well dispersed indigenous inclusions are desired and often promoted to improve the strength and toughness of weldments.

The size and population density of the inclusions are a function of the welding atmosphere, the filler and base metal composition, and the heat input. Welding processes with high Oxygen (O) and Nitrogen (N) concentrations in the weld atmosphere will undoubtedly contain large numbers of inclusions. The low concentration of O and N in TIG and MIG welding atmospheres, see Figure 2.5, should produce weldments with relatively small numbers of inclusions, as compared to other types of welding processes. It should be noted that the quantity of inclusions in TIG and MIG weldments will be significantly higher than those in cast steel. Deoxidizing elements such as Aluminum, silicon, and titanium are often added to the filler and base metal to reduce the amount of oxygen in the weldment thus improving the toughness, (Kou, 1987, p.70-82). The toughness is improved by the above elements preventing the formation of brittle FeO oxides. The deoxidation products are usually found as small well dispersed non-metallic inclusions. This is a direct result of the high cooling rates involved in the welding process, (ie; there is insufficient time for the growth and separation of the deoxidation products to occur). The weld heat input can alter the cooling rates and the degree to which deoxidization occurs and thus also influences the inclusion size and population density.

3. Hydrogen Cracking

Hydrogen cracking (sometimes called Cold cracking or Hydrogen Induced Cracking (HIC)) is a severe problem in the welding of high strength steels. For HIC to take place the following four factors must be present; hydrogen in the weld metal, high stresses, susceptible microstructure, and relatively low temperatures (-100 to 200°C). Martensitic microstructures, especially hard and brittle high carbon martensite, are extremely susceptible to hydrogen cracking. High stresses in the weldment can result from the work-piece being rigidly constrained during the welding process. Sources of hydrogen can be from the presence of atmospheric moisture, hydrated oxides, oil or grease contamination, etc. The exact mechanism for HIC is still not clearly understood, however it is known that the problem results when hydrogen diffuses from the weld metal into the HAZ prior to the HAZ austenite to martensite transformation. The susceptible of HIC can be reduced by preheating (preventing the formation of martensite), postheating (stress-relief of the weldment), or the reduction of the carbon content present (softening and/or elimination of martensite formation); (Kou, 1987, p.344-347).

4. Reheat Cracking

Reheat Cracking is a typical problem in steels containing chromium (Cr), molybdenum (Mo), and sometimes vanadium (V). Reheat cracking occurs in the HAZ during postweld stress relieving, especially in thick-section welds, where residual stresses can be severe. Since Cr, Mo, and V are strong carbide formers, it is possible that carbides can precipitate upon heating to stress-relief temperatures. The carbides would form within the HAZ grains but not at the grain boundaries. This would result in the interior of the grain being

17

relatively stronger than the grain boundaries, and thus intergranular cracks could form in an attempt to relieve the residual stresses. The susceptibility of Reheat cracking can be reduced by reducing the content of carbide formers in the weld metal and/or reducing the level of residual stresses in the weldment (ie; minimize the restraints placed on the work-piece during the welding process); (Kou, 1987, p.351-354).

E.   SCOPE OF PRESENT WORK

The high strength, high toughness, and superb weldability available in Ultra Low Carbon Bainitic (ULCB) steels makes this family of steels ideal for Naval applications.   Through extensive research, the properties required to produce high strength ULCB steels, and ULCB weldments, are well understood. However, the parameters required to produce tough ULCB weldments have been found to be very complex and as of yet not fully understood.   Thus, the present work will attempt to correlate the embrittlement of ULCB/ULCB multipass weldments to the microstructure and to the type, size, number, and distribution of the non-metallic inclusions in an attempt to gain a better understanding into the influence of theses factors on the toughness of ULCB weldments. Eleven ULCB/ULCB multipass TIG weldment and one ULCB/ULCB multipass MIG weldment samples will be utilized for this purpose.   The weldment samples vary in weld metal compositions and weld heat input.   The type, size, number, and distribution of the non-metallic inclusions will be investigated with the use of the Scanning Electron Microscope (SEM) and the microstructure investigated through optical microscopy.

18

III. EXPERIMENTAL PROCEDURE

A. SAMPLE PREPARATION

1. Initial Preparation

The Ultra Low Carbon Bainitic (ULCB) steel Charpy TIG weldment samples were supplied by the Naval Surface Warfare Center, Annapolis Detachment. The Initial preparation of the samples consisted of the following: Twenty two ULCB ingots of differing composition were manufactured. Base plates of 1.25 inch thickness and weld filler wires were cut from the center of the twenty two ULCB ingots. The base plates were TIG welded with multiple passes using filler wire of like material. Eleven of the weldments were tested to determine the final chemical composition, see Table 3.1. Twelve Charpy (and other mechanical test blanks), were cut from the hearts of each weldment for testing. The Charpy sample blanks were cut transversely to the weld path with the Charpy notches aligned to the weld metal center line, see Figure 3.1. The notches of all Charpy samples were located on the front face of the sample, as depicted in Figure 3.1, with the exception of three samples which had their notches located on the top face. The Charpy samples were tested for impact toughness prior to shipment to the Naval Postgraduate School.

The MIG welded ULCB on modified HSLA sample was supplied by the Naval Surface Warfare Center Annapolis Detachment as a sectioned multibead on plate sample. The chemical composition is listed in Table 3.1.

TABLE 3.1   SAMPLE COMPOSITION DATA

Sample	C	Mn	Si	Ni	Mo	Cr	Nb	Al	Ti	O	H
32A3-G3	.03	0.97	.18	3.43	2.48	---	.050	.015	.009	.002	---
29B4-10	.010	1.55	.16	4.58	3.24	.28	.046	.013	.006	.007	3.8
49A3-11	.012	2.15	.21	5.00	2.76	.52	.045	.020	.011	.007	6.3
49A4-9	.012	2.19	.21	5.02	2.75	.50	.043	.022	.009	.006	6.6
49B4-4	.015	2.02	.20	4.70	2.55	.51	.044	.020	.015	.006	5.3
49C3-1	.010	1.84	.15	4.75	2.44	.50	.043	.027	.011	.013	6.5
50B3-2	.010	2.07	.18	4.73	2.45	.50	.037	.020	.008	.012	5.1
50B4-2	.023	2.49	.18	5.20	2.90	.44	.034	.022	.007	.012	8.2
51B4-6	.018	2.49	.19	5.42	3.03	.48	.042	.023	.007	.010	3.5
51C2-3	---	---	----	----	----	---	---	---	---	---	---
75C3-10	.016	1.93	.19	4.99	4.96	.53	.033	.023	.008	.009	7.9
75C4-11	.014	1.86	.16	4.94	4.97	.54	.034	.022	.006	.009	4.8

NOTE: 1)   All amounts are in Weight Percent except "H" which is in ppm.

2)   32A3-G3 is for Filler Wire - Base Metal is modified HSLA 100.

3)   51C2-3 was not analyzed but should be very close to 51B4-6.

20

Weld Path

Sample

Base Metal
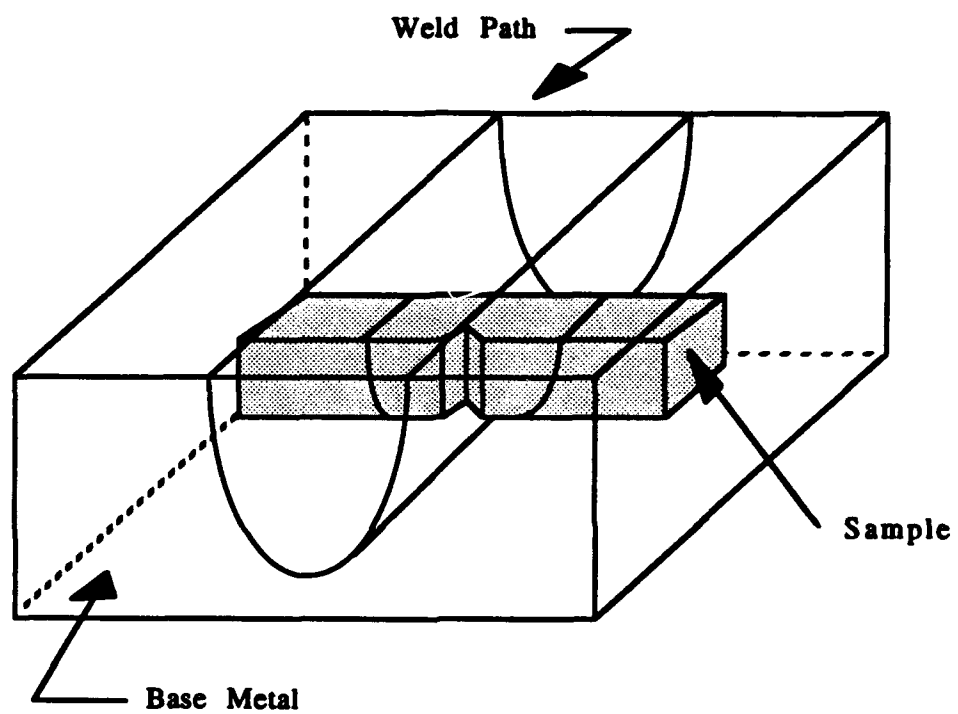
Figure 3.1   Charpy Weldment Sample Orientation

2. Preparation for Electron Microscopy

The Charpy samples were prepared for electron microscopy via the following process: A cut was made just below the fracture surface using a diamond wafer saw. This was designed to expose a flat surface with roughly the same microstructure as the fractured surface prior to impact testing. The samples were then cold mounted and ground flat using wet silicon carbide paper. Sandpaper grits were used in the order; 240, 320, 400, 600, 2400 and 4000. The cold mount material was then removed and the samples given a final polish. Polishing was performed on a polishing wheel using one micron diamond paste on a Microcloth self adhesive cloth at a wheel speed of 400 rpm.

The MIG sample was prepared using the same steps as above with the exception of cutting and the use of a cold mount.

3. Preparation for Optical Microscopy

The samples were prepared for optical microscopy by etching the surfaces, polished for electron microscopy, in a solution of 5% nital (5% nitric acid - 95% methanol) for approximately 70 seconds.

B. MECHANICAL TESTING

The Naval Surface Warfare Center Annapolis Detachment conducted all of the mechanical testing performed on the samples. This testing included Rockwell Hardness (Rc), percent elongation (El'n), reduction in area (RA), Charpy V-Notch Upper Shelf Energy (CVN USE), Fracture Appearance Transition Temperature (FATT) and other tests. The results of the above testing were recorded and forwarded to the Naval Postgraduate School.

C. ELECTRON MICROSCOPY

1. Inclusion Size and Population Density

The average size and population density of the non-metallic inclusions for each weldment was determined by examining 100 to 150 random 4000x magnification fields per sample.   For each field, of a particular sample, the number of inclusions and the size of each inclusion was recorded.   SEM micrographs depicting a typical 4000x magnification field and the measurement of an inclusion, are shown in Figures 3.2 and 3.3 respectively. The numbers and sizes were summed and then divided by the total number of fields and the total number of inclusions respectively to obtain the population density and average size for that sample.   A Cambridge Stereo Scan S200 Scanning Electron Microscope (SEM) was utilized for the above observations. The SEM was operated using a Tungsten filament with an accelerating voltage of 20 kV and a working distance of 9mm.   Further information concerning SEM and its use may be obtained in Appendix A.

2. Inclusion Composition

Twenty non-metallic inclusions per weldment sample were randomly selected for chemical analysis.   Chemical analysis was performed with the use of a KEVEX 8000 Energy Dispersive X-ray (EDX) Analysis Spectrometer in conjunction with the SEM.   The SEM was operated using a Tungsten filament with an accelerating voltage of 20 kV and a working distance of 18mm.   The inclusion compositions were recorded and averaged for each weldment sample.   Further information on the KEVEX system may be obtained in Appendix B.
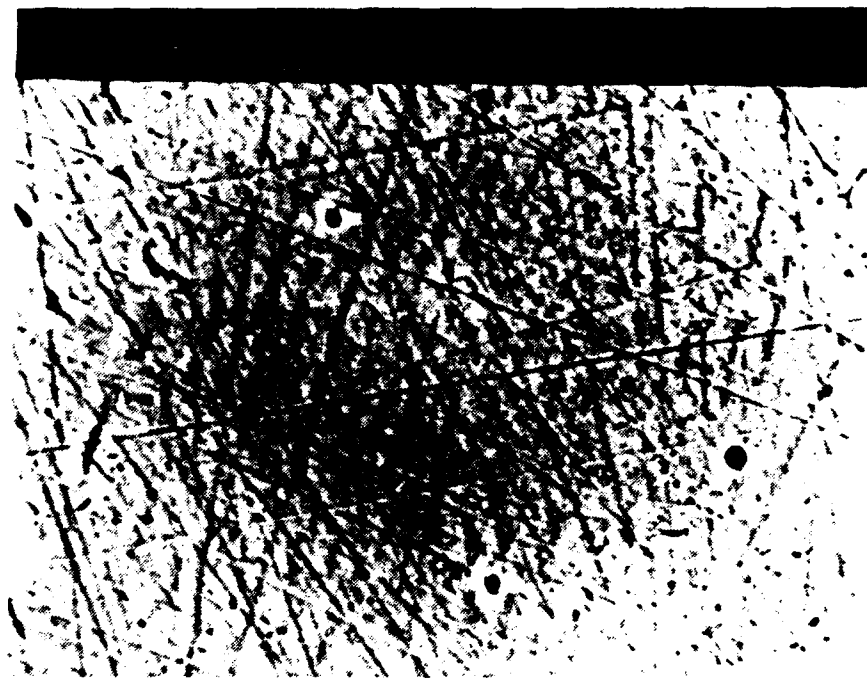
Figure 3.2 SEM Micrograph of Sample 49A3 (4000x MAG)

Figure 3.3 SEM Micrograph of Inclusion (Sample 49A3)

D. OPTICAL MICROSCOPY

A Zeiss (low Mag) Stereo microscope was used to obtain low magnification (25X - 30x) macrographs of the etched weldment samples. Oblique illumination as opposed to reflected was utilized to obtain the best macrostructure contrast.

A Zeiss ICM 405 microscope was used to obtain medium and high magnification (50x - 200x) micrographs of the etched weldment samples.

IV. RESULTS AND DISCUSSION

A. MECHANICAL TESTING

The mechanical properties and test analysis of the ULCB weldments has been previously reported (McDonald, 1992) and thus only a summery of the pertinent test results will be provided. The mechanical testing revealed that the strength of the ULCB weldments could be correlated to the alloying content by use of the "Modified" Pickering Formula[1], however the toughness varied in a complicated manner from sample to sample and could not readily be correlated with the alloying content or the welding properties (McDonald, 1992). McDonald also reported that the samples appeared embrittled with increased molybdenum content. Table 4.1 below lists the strength and toughness of the weldment samples investigated.

B. MICROSTRUCTURAL ANALYSIS

1. Inclusion Size and Population Density

The average non-metallic inclusion size and population density for each weldment sample is provided in Table 4.2. The inclusion size distribution for each weldment sample is provided in tabular format in Table 4.3 and

---

[1]"Modified" Pickering Formula:
$$T.S.(MN/m^2) = 15.4[16 + 125(C) + 15(Mn + Cr) + 12(Mo)$$
$$+ 6(W) + 8(Ni) + 4(Cu) + 25(V + Ti)]$$

TABLE 4.1 MECHANICAL TEST RESULTS

SAMPLE ID	Heat Input (kJ/in)	Yield Str. (ksi)	Tensile Str. (ksi)	CVN USE (ft-lb)	CVN +30F (ft-lb)	Weld Wire
32A3-G3	60	---	---	---	---	---
29B4-10	120	122	130	145	145	Sq. rod
49A3-11	60	125	133	120	80	Sq. rod
49A4-9	60	125	133	125	---	Sq. rod
49B4-4	100	124	137	130	73	Sq. rod
49C3-1	60	120	138	120	86	Sq. rod
50B3-2	50	122	134	80	60	1/16 Rnd
50B4-2	100	127	157	40	20	1/16 Rnd
51B4-6	100	123	157	40	27	1/16 Rnd
51C2-3	100	136	153	110	30	Sq. rod
75C3-10	100	128	147	80	30	1/16 Rnd
75C4-11	50	128	147	40	23	1/16 Rnd

NOTE: "---" indicates item was not evaluated.

27

TABLE 4.2   INCLUSION COUNT SUMMARY

SAMPLE	FIELD (4kX)	INCL	INCL/FIELD	INCL/mm^2	AVE (nm)	Q (kJ/in)
32A3-G3	100	381	3.81	7620	483	60
29B4-10	100	251	2.51	5020	308	120
49A3-11	150	311	2.02	4040	407	60
49A4-9	100	327	3.27	6540	423	60
49B4-4	100	235	2.35	4700	457	100
49C3-1	100	330	3.30	6600	362	60
50B3-2	118	243	2.00	4000	535	50
50B4-2	150	249	1.61	3220	440	100
51B4-6	116	266	2.23	4460	579	100
51C2-3	100	358	3.58	7160	382	100
75C3-10	116	197	1.64	3280	417	100
75C4-11	100	303	3.03	6060	409	50

TABLE 4.3   INCLUSION SIZE DISTRIBUTIONS

Size	Number of Inclusions per Inclusion Size (Size: microns)														
	0.1	0.2	0.3	0.4	0.5	0.6	0.7	0.8	0.9	1.0	1.1	1.2	1.3	1.4	1.5
32A3-G3	5	79	59	56	50	44	34	17	14	11	5	5	1	1	
29B4-10	13	58	108	53	17	2									
49A3-11	17	66	48	47	65	34	17	2	2	4	1	1			
49A4-9	45	65	40	42	35	40	28	14	13		1	1		1	1
49B4-4		40	72	22	23	28	21	16	8	3					
49C3-1		63	118	84˙	36	17	6	4	1		1				
50B3-2		15	57	29	36	34	25	19	7	6	2	2	1	1	
50B4-2	32	35	36	28	33	24	33	11	4	2	1	1	1		
51B4-6	1	7	30	42	62	38	30	19	10	8	5	2	2	1	1
51C2-3		38	128	106	61	15	6	2	1					1	
75C3-10	1	15	75	40	21	3	2								
75C4-11		30	96	85	56	15	13	3	2	2					

graphically in Appendix C. It was immediately noted that the average non-metallic inclusion size varied only slightly from sample to sample (0.31 - 0.58 microns), and thus the average inclusion size was not deemed a significant factor in the variation of the toughness that existed between samples. The inclusion population density was also deemed to be an insignificant factor in the variation of toughness. This later observation was based on the fact that a correlation between population density and relative toughness could not be established. For example; in comparing sample 49A3 to sample 49C3, the inclusion population density ranged from 4040 to 6600 INCL/mm^2, however there was not a significant variation in the relative toughness between the samples (CVN USE: 120 to 120 ft-lb).

The small variation in average inclusion size from sample to sample could possibly be explained as follows: If the various weldments had roughly the same number of nucleates, say TiN, previously existing in their weld metals (or less likely, if the weld pools nucleated inclusions at approximately the same rate), and if the the weld pools had roughly the same quantity of dissolved oxygen, than the non-metallic inclusions could only grow to approximately the same size given the very rapid cooling process. The above could also explain why changes in factors such as welding methods, heat input, and base and weld wire compositions had little or no apparent effect on the average size or population density of the inclusions.

In general terms, the inclusions present within the samples investigated were of a size (< 1 - 2 microns) to be classified as being beneficial to the toughness of the samples, (ie; large enough to nucleate grains and block excessive grain growth, yet small enough not to act as crack initiation sites).

29

To this extent, the inclusions were of sufficient size (>0.2 microns) to promote the nucleation of acicular ferrite (Kiessling, 1989, p.106), a microstructure desired in welding for its ability to promote toughness. However in TIG welding the amount of oxygen in the weld metal is so low as to preclude the formation of sufficient numbers of inclusions such that significant amounts of acicular ferrite are not formed.

2. Inclusion Composition

All of the inclusions identified were spherical, complex manganese-aluminum-silicates. The average inclusion chemical composition for each sample is listed in Table 4.4. Compositions of the individual inclusions analyzed is provided in Appendix D. The last three columns in the Appendix D tables (under the "Oxide % w/o TiO_2" headings), were used to plot the inclusion chemical compositions on $MnO-SiO_2-Al_2O_3$ Phase diagrams, Appendix E. The last three columns were derived by assuming that the TiO_2 acted as the nucleation sites for the inclusions and otherwise did not react with the $MnO-SiO_2-Al_2O_3$ oxides. This was assumed because of the significantly higher melting temperature of TiO_2 oxides. It is more likely that the Ti formed TiN, (TiO_2 was assumed to simplify the KEVEX analysis). This is not significant, because like TiO_2, TiN has a high melting temperature and thus should not react with the oxides.

The variations in the non-metallic inclusion compositions, can be explained by the amount of available oxygen in the weld atmosphere. As was seen in Figure 2.6, the TIG welding process shields the weld pool from oxygen more efficiently than does the MIG welding process. If a relatively small amount of oxygen is available, as is the case in a "clean" TIG weld, the

30

TABLE 4.4   AVERAGED INCLUSION CHEMICAL COMPOSITION

Sample	Weight Percent (%)				Oxide Percent (%)				Oxide % w/o TiO2		
	Al	Si	Ti	M n	Al2O3	SiO2	TiO2	MnO	Al2O3	SiO2	MnO
32A3-G3	5.42	30.91	3.27	59.80	8.56	50.38	4.56	36.58	9.0	52.7	38.3
29B4-10	26.48	8.08	23.34	41.99	30.29	16.61	28.25	24.84	45.3	17.6	36.1
49A3-11	50.81	0.74	12.25	35.96	48.49	1.68	16.09	33.25	57.9	2.2	39.9
49A4-9	60.40	0.39	7.30	32.00	61.39	0.43	9.04	29.41	66.7	0.5	32.7
49B4-4	42.88	0.99	20.50	35.38	44.61	2.25	24.45	28.69	58.2	3.4	38.4
49C3-1	35.88	0.53	25.52	38.02	40.24	1.35	30.32	28.09	57.8	2.0	40.3
50B3-2	27.01	9.17	13.45	50.36	33.82	18.31	19.05	28.83	41.7	22.7	35.5
50B4-2	21.59	19.07	7.44	51.91	25.53	33.93	10.82	29.71	28.9	37.8	33.3
51B4-6	17.59	8.66	9.84	63.52	23.96	16.70	13.73	43.42	30.0	19.3	50.7
51C2-3	18.36	15.69	12.56	53.29	25.49	28.76	17.36	28.40	30.8	34.7	34.4
75C3-10	14.98	18.84	9.83	56.61	20.73	32.01	13.62	33.64	24.7	35.9	39.4
75C4-11	13.02	11.07	15.30	60.61	19.99	22.41	20.43	37.17	25.4	27.4	47.2

aluminum will react with the majority of the oxygen and thus form inclusions with compositions similar to Galaxite ($MnO-Al_2O_3$). This is due to the Al being the strongest deoxidizing element in the weldments. When the amount of available oxygen is larger, as in MIG welding, the relative amount of Al_2O_3 decreases and the relative amount of SiO_2 increases, thus inclusions form with compositions similar to Rhodonite ($MnO-SiO_2$). This is a result of the Al being quickly "burned out" by the formation of oxides and possibly removed in the slag. Intermediate levels of available oxygen and the $MnO-SiO_2-Al_2O_3$ oxide compositions discussed above are presented schematically in Figure 4.1.

Based on the previous discussion, the 49xx samples represent "clean" TIG weldments, sample 32A3 a typical MIG weldment, and the other samples fall between these two extremes,(as far as the relative shielding of Oxygen from the molten weld metal is concerned). Reviewing Tables 3.1, 4.1, 4.2, and 4.3 revealed that the above had little appreciable effect on the oxygen content, the toughness, or the inclusion size, population density, and distribution of the various samples. Thus the variation in the toughness, that existed between the weldment samples, can not be correlated with these results.
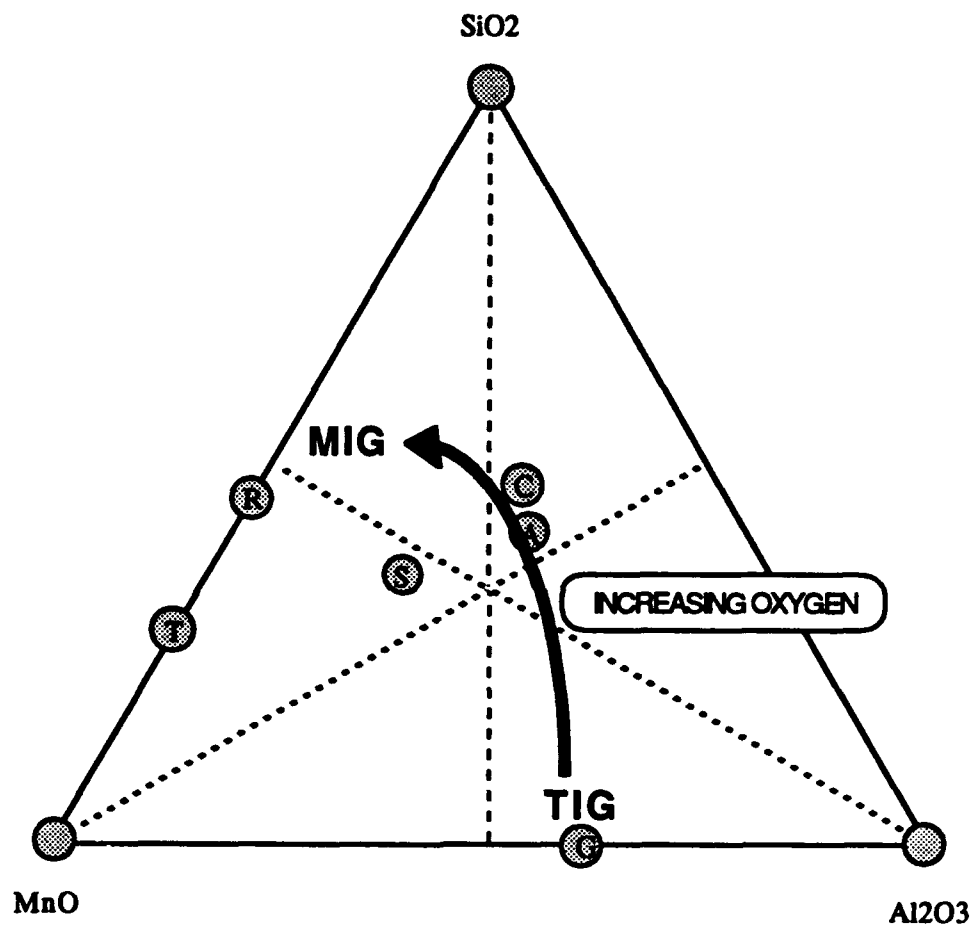
Figure 4.1   Inclusion Composition vs Welding Method

3. Weld Metal Microstructure

a. Grain Zone Bands

As previously reported (McDonald,1992), the samples consisted mostly of bainitic microstructures with varying degrees of columnar, coarsened, and refined grains present. This investigation found that the above microstructures appeared as bands running through the Charpy weldment samples. A schematic representation of these grain zone bands is provided in Figure 4.2. Micrographs of the weldment samples, clearly showing these bands, can be found in Appendix F; (Take note that the sample face which contained the Charpy V-Notch is located at the bottom of the figures). It was determined that the type and quantity of these grain zone bands were the predominant factor in the variation of the toughness between samples, (ie; a sample with a large of number refined grain zones should be significantly tougher than a sample with fewer bands of larger grains). A prime example of this follows: Samples 51B4-6 and 51C2-3 had nearly identical weld metal compositions and heat inputs, Yet series 51C2 had a CVN USE 2.68 times larger than series 51B4. The reason for this large variation, between samples which should have yielded similar results, can be explained by the fact that sample 51B4-6 had a band of (weak) Columnar grains spanning nearly half of the sample, see Figure F.8, whereas sample 51C2-3 had more numerous bands of relatively smaller grains, see Figure F.9. Similar correlations between the toughness and the type and size of the grain zone bands can be made for the other weldment samples.

34
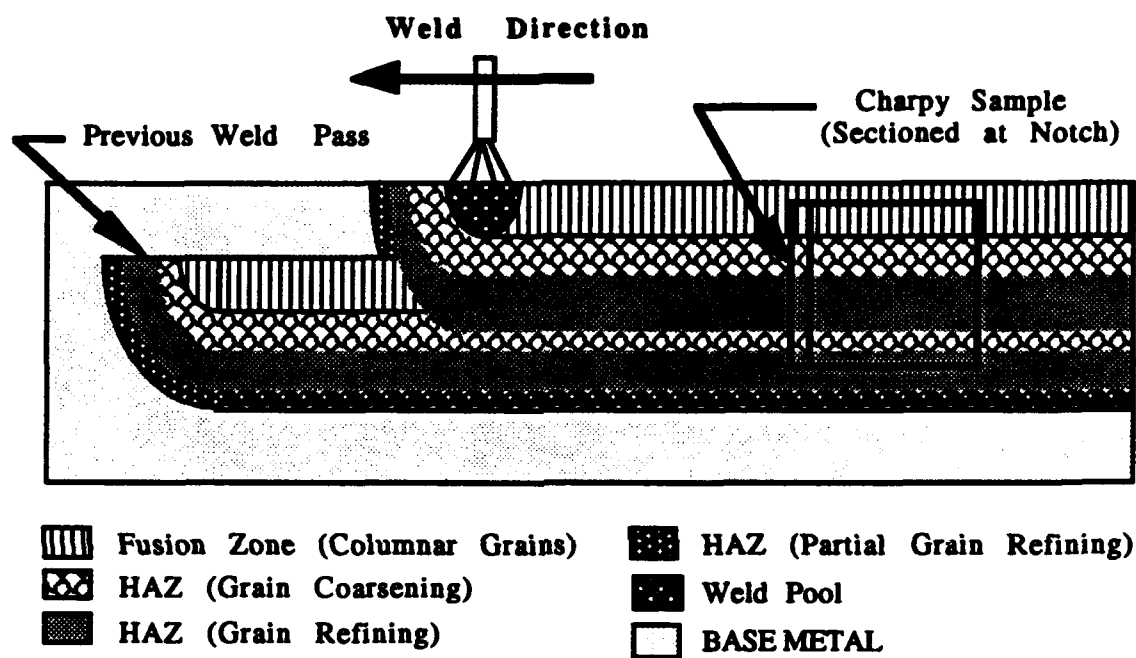
Figure 4.2 Charpy Sample Weld Grain Schematic

The factors which strongly effect the size and location of the grain zone bands are; the multipass weldment geometry (ie; weld bead overlap, bead placement, order of bead weldment, etc.), the relative location of the Charpy sample within the weldment, the weld heat input, and the weld metal composition. These parameters must be accounted for and or more strictly controlled if accurate comparisons of mechanical testing of multipass weldments are to be made. It is thus felt, that the alloying and welding parameters used in this study should be reevaluated under the above guidelines in order to obtain a better understanding of their true effects in ULCB multipass weldments.

b. Transgranular Cracking

When the ULCB Charpy weldment samples were viewed under the high power optical microscope all of the samples contained arc shaped boundaries integral to the microstructure. The orientation of these boundaries indicated that they must have been formed by the "stepped" solidification of the back of the weld pool as it traversed the material. A schematic diagram of this process is provided in Figure 4.3. In the majority of the samples a distinctive change in grain size occurred across the boundaries, see Figure 4.4. The change in grain size could possible have resulted from a process similar to that of HAZ Grain Coarsening, (ie; the grains directly behind the weld pool solidification boundary grew and coarsened while the material in front of the boundary was still in the molten state). This theory is supported by the fact that the enlarged grains are on the convex side of the boundary, (similar to the location of the HAZ Grain Coarsening zone in relation to the Fusion Zone). A deviation in the above was observed in samples

36

75C3-10 and 75C4-11. In these samples the solidification boundaries appeared to be transgranular and grain coarsening across the boundaries did not appear to have taken place, see Figure 4.5. When the 75XX samples were viewed under higher magnification the boundaries were found to be cracks and/or cracks were found running parallel to the boundaries, see Figure 4.6. Sample 75C3 was re-cut, polished, and etched to expose a microstructure surface 5 mm away from the original fractured surface. This was done to determine if the cracks existed prior to the impact test or if they resulted from the impact test. As seen in Figure 4.7, cracks were again identified. The location and orientation of these cracks were nearly identical to the cracks on the surface closer to the fracture surface. This would indicate that the cracks were one and the same.

The cracks found, at the solidification boundaries in the 75XX samples, provide an explanation for the increase in embrittlement of the weldment samples with increasing amounts of Molybdenum (Mo) alloying previously discovered, (McDonald, 1992). The 75XX samples contained nearly double the Mo (4.96 Wt%) of the other weldment samples. It is believed that the relatively large quantity of Mo allows the formation of a brittle Mo phase. One possibility is that it could form with Carbon (C) despite the extremely low weight percent of C (< 0.025 Wt%). Another is the formation of a brittle FeMo intermetallic compound such as "R" or Lambda intermetallic, see Figure 4.8. There is a considerable amount of restraint placed on the welds within the multipass weldments thus large stress fields would be generated upon the solidification of the weld pools. During subsequent weld passes these stress fields could be relieved by the formation of cracks through the brittle Mo

Weld Direction

Previous Weld Passes

Charpy Sample
(Sectioned at Notch)

Solidification Boundary
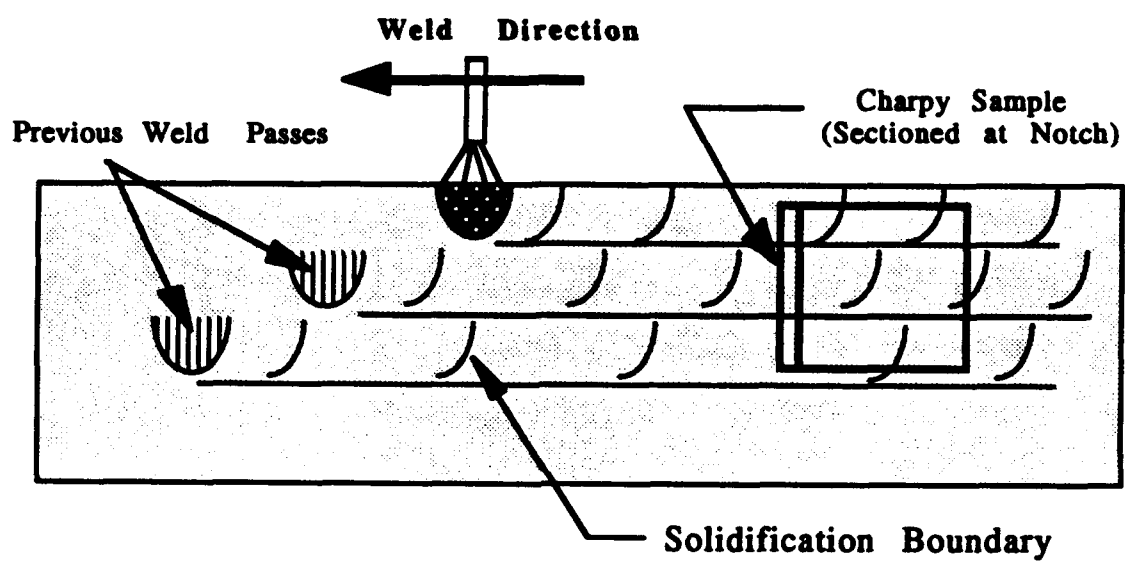
Figure 4.3   Weld Pool Solidification Boundaries
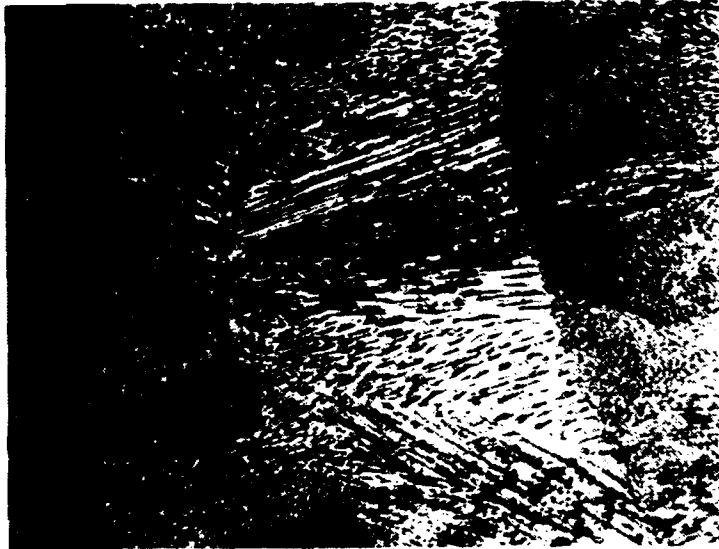
Figure 4.4 **Optical Micrograph of 51B4-6 (50x)**
(Weld Pool Solidification Boundary)

Figure 4.5 **Optical Micrograph of 75C3-10 (100x)**
(Transgranular Solidification Boundary)

Figure 4.6 **Optical Micrograph of 75C3-10 (200x)**
(Solidification Boundary - Original Surface)

Figure 4.7 **Optical Micrograph of 75C3-10 (200x)**
(Solidification Boundary - 5 mm from Fractured Surface)

40
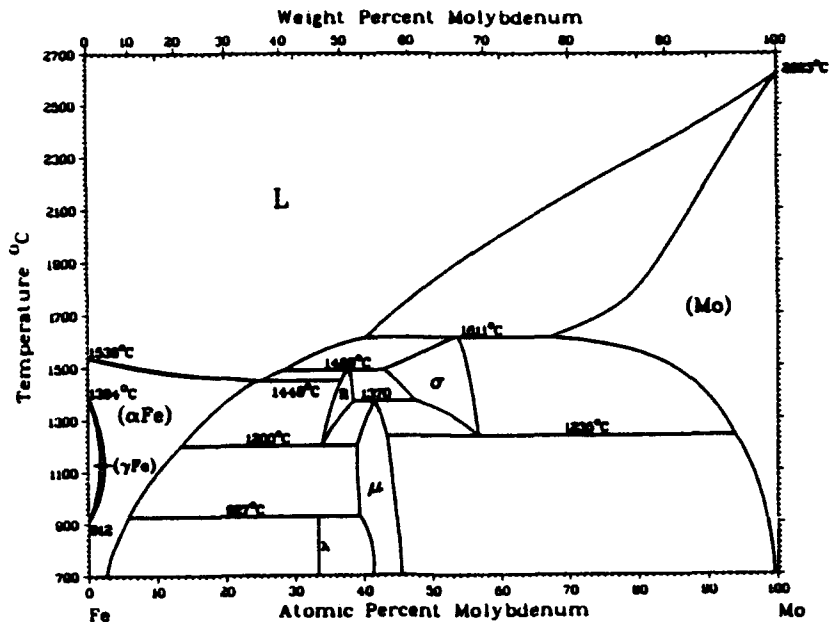
Figure 4.8   FeMo Phase Diagram

(ASM   International,   1990,   p.1727)

phase, possible in a process similar to that of reheat cracking. Corrosion- and heat-resisting low-alloy steels are said to be susceptible to reheat cracking if CS (Crack Susceptibility) in the following equation is greater than one, (Kou, 1987, p.351):

$$CS = \%Cr + 3.3(\%Mo) + 8.1(\%V) - 2$$

For the 75XX samples, CS is significantly greater than one (CS = 14.37). The cracks are not thought to be HIC (or cold cracking) due to the fact that the other weldment samples contained similar levels of hydrogen, Table 3.1, and yet crack formation at the solidification boundaries in these samples was not present.

V. SUMMARY

A. CONCLUSIONS

1. Inclusions

The majority of the nonmetallic inclusions identified were spherical, complex manganese-aluminum-silicates. The sizes of the inclusions ranged from 0.10 to 2.3 microns with the average inclusion size per sample ranging from 0.31 to 0.58 microns. The population density of the inclusions per sample ranged from 3220 to 7620 inclusions per square millimeter. The nonmetallic inclusions were deemed not to be a significant factor in the variation of the toughness that existed between the samples investigated. This determination was based on the fact that there was not a significant variation in the average size, distribution density, or chemical composition of the nonmetallic inclusions in samples with high toughness values versus those samples with low toughness values.

2. Microstructure

The microstructure was determined to be the major contributing factor in the varying degrees of toughness between otherwise like samples. Significant differences were observed in the size, quantity, and location of various grain (columnar, coarsened, and refined) zones within these samples. The differences encountered can be directly attributed to the complexity and nonuniformity of multipass weld metal geometries. Without a precise means of manufacturing a reproducible multipass weld metal geometry and/or without the use of a very large number of Charpy samples (with random Charpy notch

42

placement relative to weld metal center line) the toughness between weld metal samples with different degrees of alloying, heat input, etc. can not be accurately compared and thus an optimum combination of these properties cannot be readily determined.

The increase in weld metal embrittlement with an increase in molybdenum (Mo) alloying would appear to be due to the formation of transgranular cracks located directly behind solidification boundaries generated as the weld pool traverses the work piece. It is believed that the relatively high weight percent of Mo (2.5 to 5.0 Wt %) allows the formation of a brittle Mo phase. One possibility is theat it could form with carbon (C) despite the extremely low weight percent of C (< 0.025 Wt %). Another possibility being, the formation of a brittle FeMo intermetallic compound such as "R" or Lambda intermetallic. Due to the weldment being rigidly constrained large stress fields would be generated within the weld metal. During subsequent weld passes these stress fields could be relieved by the formation of cracks through the brittle Mo phase, possibly something akin to reheat cracking.

B. RECOMMENDATIONS FOR FUTURE STUDY

The means to more accurately conduct impact toughness testing of multipass weldments must be investigated to alleviate the current inconsistences in the process. This investigation should include a study into the possibility of designing a process which more consistently "lays down" multipass weld beads so that relatively uniform and relatively reproducible multipass weld metal Charpy impact samples can be manufactured.

43

A process of this nature would allow for a more precise comparison of various weldment variables on toughness to be made as well as facilitate the investigation of the properties that would lead to maximizing the desired microstructures in multipass weldments.

The effects of the various alloys on the strength and toughness of ULCB weldments should be studied in further detail to attempt to obtain an optimum base and weld wire composition. This study should further investigate the complicated nature in which the alloys used in ULCB steels interact within the weld metal. In particular, alloying with Mo and its effects on weldment embrittlement when used in quantities of greater than two weight percent should be studied in detail.

APPENDIX A

SCANNING ELECTRON MICROSCOPY

The Scanning Electron Microscope (SEM) was used extensively for the determination of the size and distribution of the nonmetallic inclusions. The composition of the nonmetallic inclusions was evaluated using the SEM in conjunction with the KEVEX analyzer. The SEM modes of operation that were utilized are described below.

Secondary Electron (SE) Mode provides topographical information of the sample. Topographical information is generated by, the SEM, rastering high voltage electrons across the samples surface. The incident high voltage electrons eject lightly bound low energy valence electrons (or secondary electrons) from the atoms within the sample. Due to the low energy of the secondary electrons only those generated near the immediate surface of the sample can escape. For this same reason, high spots on the sample appear as bright objects and low regions will appear as dark ones. Materials with relatively high atomic numbers appear lighter than elements with lower atomic numbers due to the lower energy required to remove valance electrons. Objects with low conductivity or which are not properly grounded shall also appear as bright objects due to the retention of electrons of the incident beam. The SE electrons which escape the surface are electromagnetically bent and collected on the SE detector (or Scintillator). This process generates a signal which can then be reproduced on a CRT for display.

Backscattered Electron (BSE) Mode allows the operator to more readily investigate the various phases present within a sample. The BSE image is generated by the incident high voltage electrons undergoing an elastic, or nearly elastic, collision with the nuclei of the atoms of the sample material and thus the electrons are reflected "back" towards the electron source. The BSEs are collected by the BSE detector which generates a signal that can be displayed on the SEMs CRT. BSEs are higher in energy than SEs and thus can escape from deeper within the sample. Atoms with relatively higher atomic numbers will appear brighter than ones with relatively lower atomic numbers. This is due to the larger size (and thus a larger positive charge) of the nuclei, of the higher atomic number atoms, increasing the probability of backscattering the incident electrons. The above makes the BSE Mode vital for the detailed examination of nonmetallic inclusions in steel.

Mixed Mode allows for the mixing of SE and BSE signals so that the optimum representation of the samples topographical and phase properties can be obtained.

The SEM In conjunction with the KEVEX analyzer was utilized to perform energy dispersive x-ray analysis on the nonmetallic inclusions. In this mode characteristic x-rays given off from the inclusions were detected and analyzed to determine the identity and the relative quantity of the elements present. Characteristic x-rays are produced when an incident high energy electron ejects an electron from a lower energy shell of an atom within the inclusion. An electron from a higher shell must fill this vacancy, and to do so, the electron must give off energy. The energy given off is in the form of an x-ray which is characteristic of the host atom.

APPENDIX B

ENERGY DISPERSIVE X-RAY SPECTROSCOPY

The elements and the relative quantity of the elements present in a sample may be determined by the examination of the characteristic x-rays given off by the sample when the sample is subjected to an incident beam of high energy electrons. This process is known as Energy Dispersive X-Ray Spectroscopy and is possible using the SEM in conjunction with the KEVEX analyzer. The above process was utilized to chemically analyze the nonmetallic inclusions within the subject samples and is described below.

The SEM is used to irradiate the target sample with a beam of high energy electrons, (on the order of 20 kV). An electron of sufficient energy can eject an electron from the lower shell of the target atom leaving the atom in an unstable energy state. The lower shell vacancy must be filled with an electron from an upper shell for the atom to return to a stable energy state. An upper shell electron must give off energy in order to drop to the lower energy shell. This energy is in the form of an x-ray which is of an energy level that is unique to the host atom. The x-rays are detected by a probe, within the SEM, which sends a signal to the KEVEX analyzer. The probe can only record a specific number of x-rays in any given time and this must be taken into account when performing spectral analysis. For evaluating the nonmetallic inclusions an x-ray count rate of 2000 cps for a period 80 seconds was utilized. This resulted in a "dead time" of approximately 20 percent for the

47

detector. The probe signal is manipulated by the KEVEX analyzer to provide qualitative and quantitative data on the elements present within the sample.

X-rays can travel a significantly greater distance through a sample than SE or BSE electrons. This results in poor spatial resolution of x-ray analysis. In order to overcome this draw back the following was performed. An x-ray spectrum of an inclusion was obtained by locking the incident electron beam on to a "spot" on the inclusions surface. This spectrum contains x-ray counts from the inclusion and the background matrix due to the above mentioned poor resolution problem. Next a spectrum of the local background matrix was obtained by rastering the electron beam over a given area. The matrix counts are then "stripped" from the inclusion spectrum via performing a "stripping" routine provided by the KEVEX software. This routine normalizes the two spectra and then subtracts the matrix spectrum from the inclusion spectrum leaving an accurate depiction of the inclusion chemical composition.

A second limitation to energy dispersive analysis is that light elements (below $Z=11$), are difficult to detect. Light elements more readily produce Auger electrons than x-rays when the atom is excited. The x-rays that are produced from light elements are very low in energy and have difficulty penetrating the probe window and thus are not easily detected. To overcome this problem, the KEVEX analysis provides the ability to determine the percent of light elements using stoichiometric calculations. This feature was utilized to determine the oxide compositions of the nonmetallic inclusions given the weight percent of the elements measured.

APPENDIX C - INCLUSION FREQUENCY vs SIZE CHARTS

32A3-G3 INCLUSION FREQUENCY vs SIZE
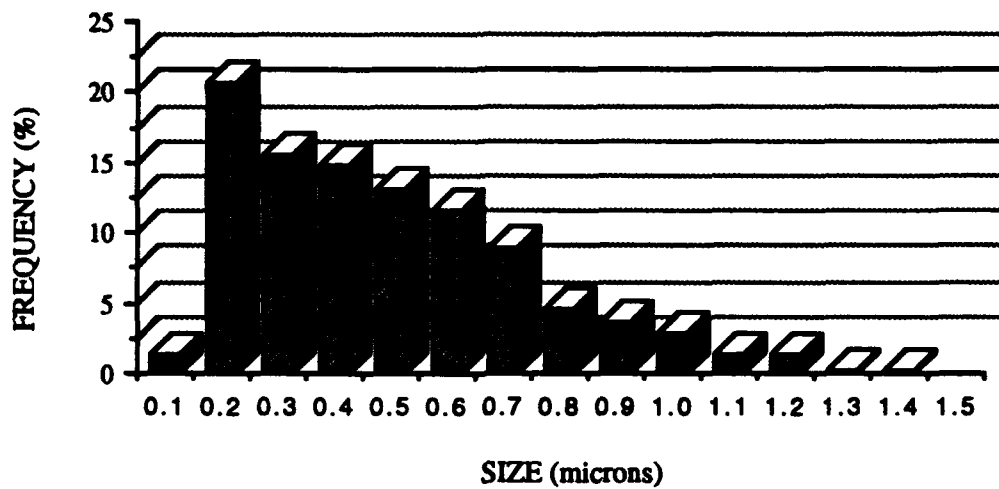
Figure C.1

29B4-10 INCLUSION FREQUENCY vs SIZE

Figure C.2

49
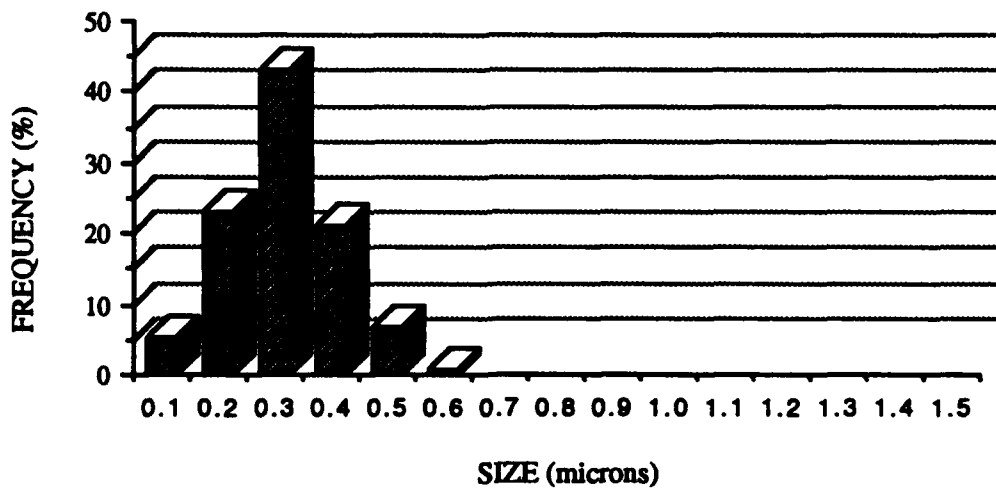
49A3-11 INCLUSION FREQUENCY vs SIZE
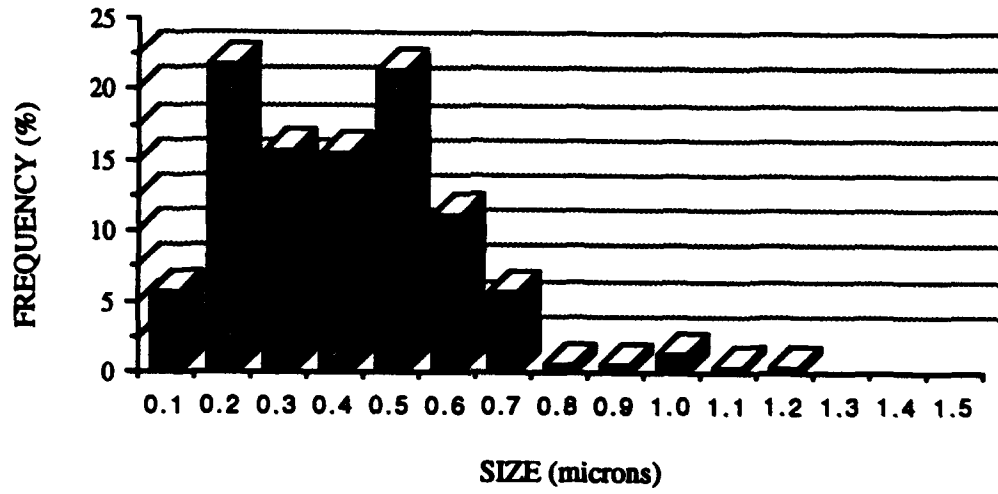
Figure C.3

49A4-9 INCLUSION FREQUENCY vs SIZE
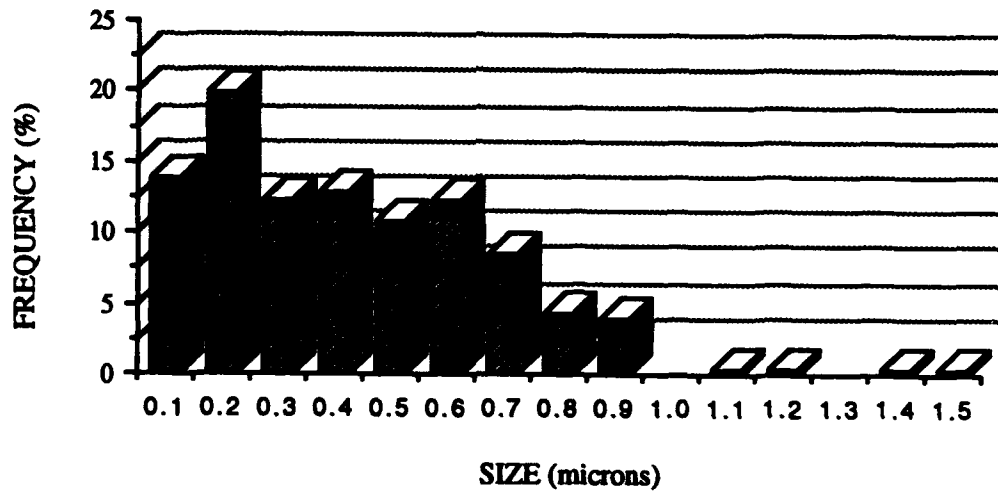
Figure C.4

49B4-4 INCLUSION FREQUENCY vs SIZE
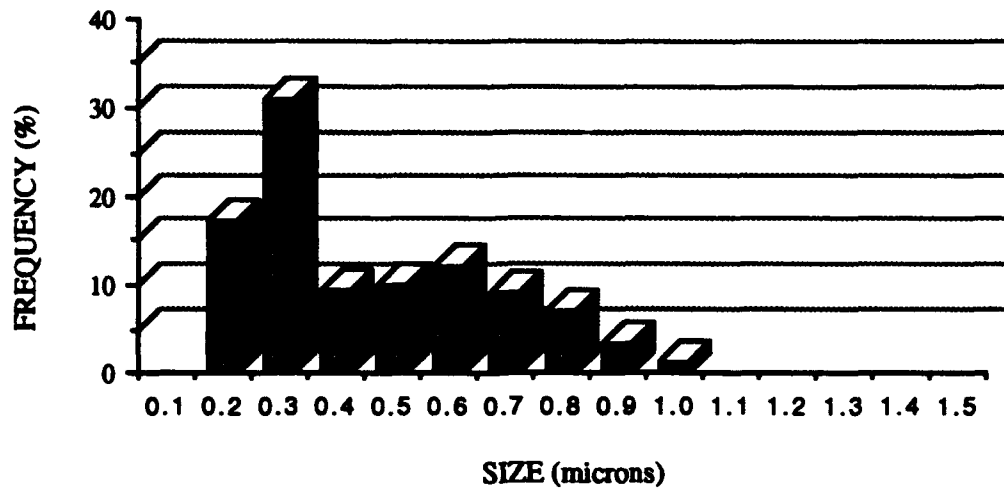
Figure   C.5

49C3-1 INCLUSION FREQUENCY vs SIZE

Figure   C.6

51
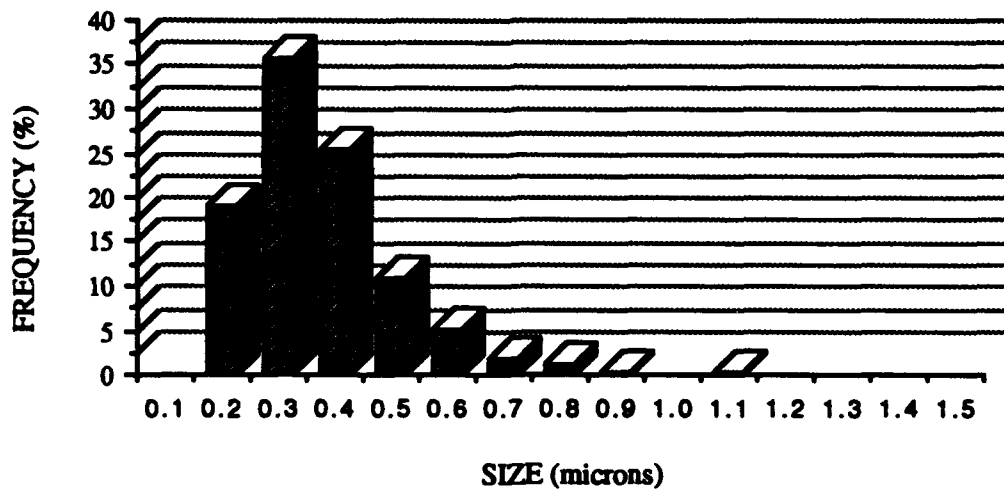
50B3-2 INCLUSION FREQUENCY vs SIZE

Figure   C.7

50B4-2 INCLUSION FREQUENCY vs SIZE

Figure   C.8

51B4-6 INCLUSION FREQUENCY vs SIZE

Figure   C.9
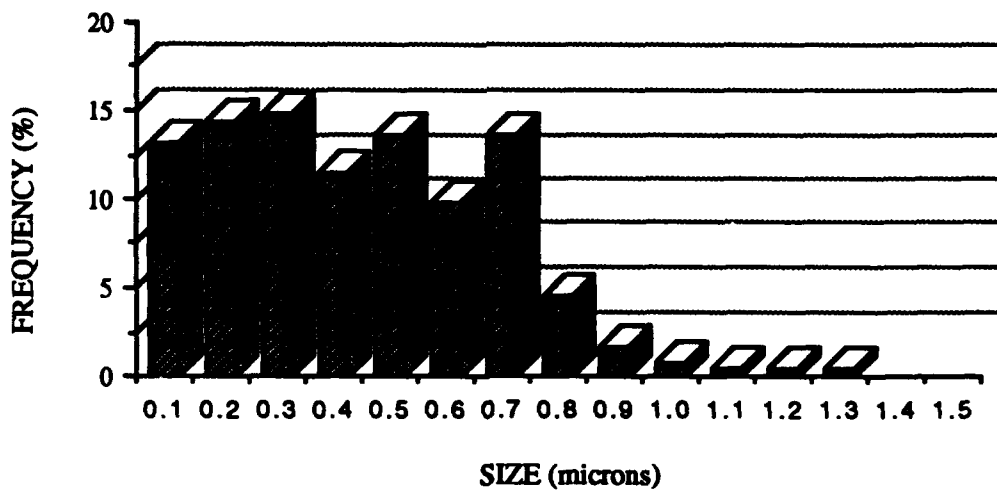
51C2-3 INCLUSION FREQUENCY vs SIZE
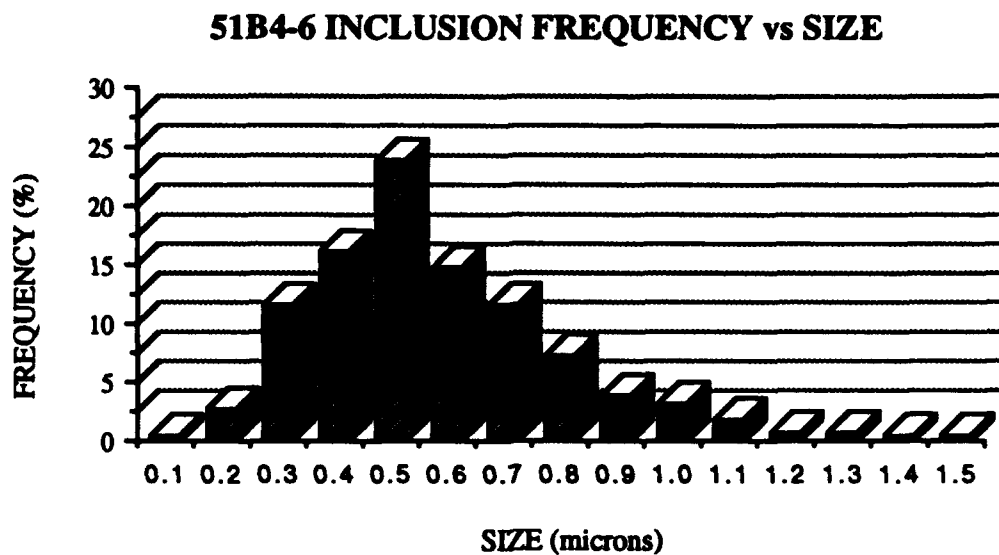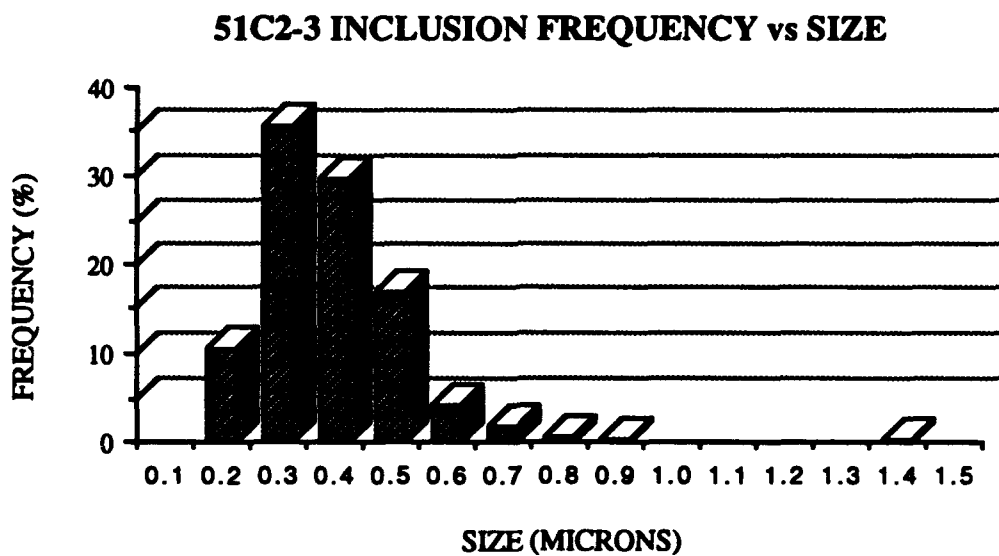
Figure   C.10

75C3-10 INCLUSION FREQUENCY vs SIZE
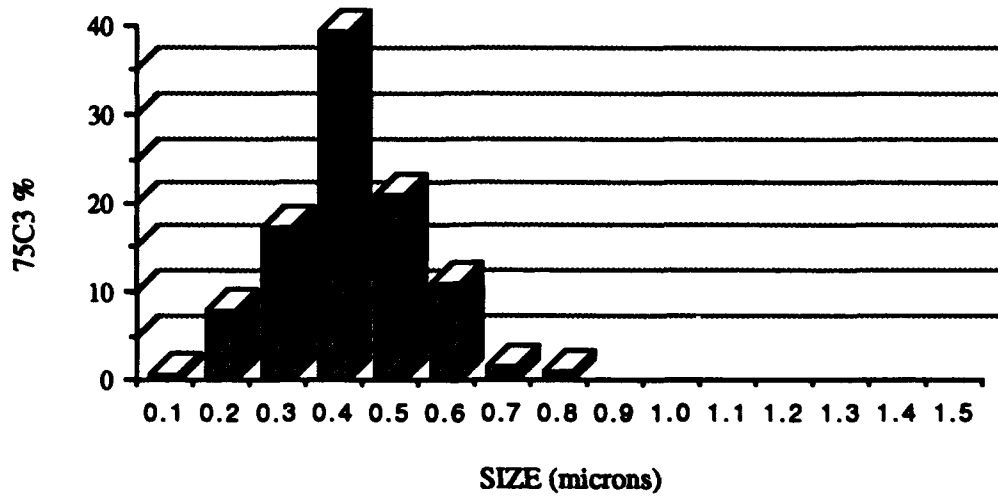
Figure C.11

75C4-11 INCLUSION FREQUENCY vs SIZE
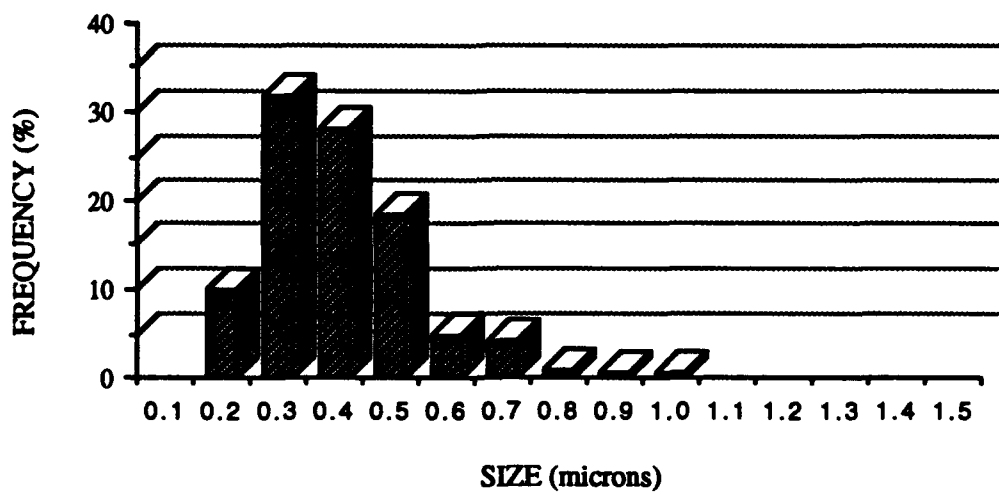
Figure C.12

APPENDIX D - INCLUSION CHEMICAL COMPOSITION

TABLE D.1   32A3-G3 INCLUSION CHEMICAL COMPOSITIONS

SAMPLE: 32A3-G3 MIG (Q: 60 kj/in)										
Weight Percent (%)				**Oxide Percent (%)**				**Oxide % w/o TiO2**		
Incl	Al	Si	Ti	Mn	Al2O3	SiO2	TiO2	MnO	Al2O3	SiO2	MnO
1	2.94	27.82	3.29	56.99	4.34	48.09	4.26	43.31	4.5	50.2	45.2
2	4.91	25.14	3.27	66.68	7.24	44.32	4.28	44.17	7.6	46.3	46.1
3	11.79	41.75	2.86	43.89	24.13	44.54	4.44	26.88	25.3	46.6	28.1
4	6.72	35.18	4.59	53.52	11.06	51.39	6.52	31.02	11.8	55.0	33.2
5	4.18	28.87	2.57	64.58	6.07	49.89	3.38	40.86	6.3	51.5	42.2
6	6.37	22.38	3.40	67.65	9.42	40.47	4.45	45.67	9.9	42.4	47.8
7	5.14	26.74	3.06	65.05	7.49	46.97	5.03	41.51	7.8	48.9	43.3
8	3.42	33.16	4.13	59.27	5.03	55.10	5.57	34.31	5.3	58.3	36.3
9	6.12	32.41	3.70	57.76	9.03	53.37	5.06	32.55	9.5	56.2	34.3
10	5.65	32.40	2.97	59.01	8.16	54.25	3.96	33.60	8.5	56.5	35.0
11	3.62	30.85	3.42	62.11	5.22	52.90	4.55	37.32	5.5	55.4	39.1
12	6.72	40.62	1.83	50.83	12.26	53.03	2.69	32.01	12.6	54.5	32.9
13	6.76	31.37	2.42	57.48	12.62	52.24	3.32	31.82	13.1	54.0	32.9
14	7.42	29.24	2.70	60.64	10.44	51.32	3.62	34.83	10.8	53.1	36.1
15	5.34	32.31	3.83	58.52	7.80	53.84	5.20	33.17	8.2	56.8	35.0
16	6.05	26.67	3.99	63.29	8.74	47.28	5.29	38.70	9.2	49.9	40.9
17	5.06	29.90	4.46	60.58	7.26	51.85	5.96	34.92	7.7	55.1	37.1
18	3.34	28.40	3.54	64.72	4.90	49.18	4.65	41.27	5.1	51.6	43.3
19	2.92	33.17	2.65	61.05	4.24	55.69	3.82	36.28	4.4	57.9	37.7
20	3.96	29.90	3.87	62.27	5.73	51.88	5.14	37.48	6.0	54.6	39.4
AVE	5.42	30.91	3.27	59.80	8.56	50.38	4.56	36.58	9.0	52.7	38.3
SUM	99.40				99.78				100.0		

TABLE D.2   29B4-10 INCLUSION CHEMICAL COMPOSITIONS

	SAMPLE:		29B4-10	TIG (Q: 120 kj/in)						
	Weight Percent (%)				Oxide Percent (%)				Oxide % w/o TiO2		
Incl	Al	Si	Ti	Mn	Al2O3	SiO2	TiO2	MnO	Al2O3	SiO2	MnO
1	29.61	2.63	27.02	40.69	36.31	6.88	31.99	24.81	53.4	10.1	36.5
2	43.18	12.68	12.21	31.94	32.33	27.16	18.42	22.10	39.6	33.3	27.1
3	43.18	12.68	12.21	31.94	31.71	18.63	27.98	21.67	44.0	25.9	30.1
4	21.58	8.89	25.60	43.94	30.40	21.47	27.13	21.00	41.7	29.5	28.8
5	15.22	12.49	27.93	44.35	23.38	28.36	27.20	21.06	32.1	39.0	28.9
6	9.38	6.99	31.33	52.31	15.68	15.09	38.21	31.02	25.4	24.4	50.2
7	18.51	12.01	19.17	50.30	26.88	26.65	25.05	21.43	35.9	35.6	28.6
8	27.05	3.83	24.08	45.05	35.49	9.60	30.65	24.26	51.2	13.8	35.0
9	16.61	10.40	27.03	45.96	25.65	24.14	28.29	21.91	35.8	33.7	30.6
10	26.22	14.48	22.69	36.60	27.16	30.03	23.98	18.56	35.9	39.6	24.5
11	40.57	4.48	18.29	36.66	36.73	10.96	27.19	25.10	50.5	15.1	34.5
12	21.09	18.73	23.51	36.67	27.04	30.61	23.87	18.48	35.5	40.2	24.3
13	17.82	19.21	17.87	45.09	26.50	31.20	23.46	18.84	34.6	40.8	24.6
14	15.48	4.28	21.59	56.65	25.74	9.86	28.58	35.83	36.0	13.8	50.2
15	46.89	4.78	9.63	38.70	43.96	11.46	14.54	30.04	51.4	13.4	35.2
16	9.78	8.63	28.30	53.29	16.03	18.49	35.47	30.01	24.8	28.7	46.5
17	15.28	1.09	45.20	38.44	27.43	2.74	39.41	30.43	45.3	4.5	50.2
18	26.17	2.49	29.17	42.17	36.43	6.50	32.17	24.91	53.7	9.6	36.7
19	43.88	0.61	25.25	30.26	38.50	1.52	33.67	26.31	58.0	2.3	39.7
20	42.10	0.31	18.78	38.80	42.43	0.82	27.75	29.00	58.7	1.1	40.1
AVE	26.48	8.08	23.34	41.99	30.29	16.61	28.25	24.84	45.3	17.6	36.1
SUM	99.89				99.99				99.0		

56

TABLE D.3   49A3-11 INCLUSION CHEMICAL COMPOSITIONS

SAMPLE:			49A3-11		TIG	(Q: 60 kj/in)					
	Weight	Percent	(%)		Oxide	Percent	(%)		Oxide	% w/o	TiO2
Incl	Al	Si	Ti	Mn	Al2O3	SiO2	TiO2	MnO	Al2O3	SiO2	MnO
1	50.45	1.23	16.43	31.89	44.62	2.73	22.19	30.47	57.3	3.5	39.2
2	57.72	0.57	10.40	31.31	54.90	1.15	13.20	30.75	63.2	1.3	35.4
3	53.02	0.64	17.63	28.72	46.07	1.33	22.61	29.99	59.5	1.7	38.8
4	58.41	0.00	12.24	29.36	55.70	0.00	15.33	28.98	65.8	0.0	34.2
5	47.91	0.00	14.01	38.08	47.15	0.00	20.63	32.22	59.4	0.0	40.6
6	50.75	0.00	18.20	31.05	45.01	0.00	24.30	30.70	59.5	0.0	40.5
7	40.17	3.51	18.59	37.73	37.91	8.71	27.47	25.91	52.3	12.0	35.7
8	58.60	1.81	6.92	32.67	56.51	3.60	8.82	31.68	61.6	3.9	34.5
9	50.68	0.38	13.51	35.49	47.73	0.22	18.78	32.81	59.1	0.2	40.6
10	45.45	1.90	13.88	38.77	43.95	4.85	21.17	30.03	55.8	6.2	38.1
11	38.41	1.70	12.48	47.40	45.78	4.48	16.55	31.24	56.2	5.5	38.3
12	28.72	1.77	25.09	44.43	37.55	4.54	32.24	25.57	55.5	6.7	37.8
13	61.89	0.00	6.58	31.53	62.39	0.00	8.20	29.41	68.0	0.0	32.0
14	67.45	0.00	5.06	27.50	69.71	0.00	6.00	24.28	74.2	0.0	25.8
15	55.37	0.74	9.67	34.22	51.99	1.55	12.62	33.24	59.9	1.8	38.3
16	57.57	0.00	8.54	34.05	56.10	0.00	10.61	33.56	62.6	0.0	37.4
17	56.17	0.47	7.17	34.50	55.55	0.52	2.55	35.55	60.6	0.6	38.8
18	55.51	0.00	8.51	35.98	55.25	0.00	11.50	32.56	62.9	0.0	37.1
19	51.55	0.00	9.95	35.10	30.82	0.00	11.43	57.25	35.0	0.0	65.0
20	30.38	0.00	10.18	59.48	25.13	0.00	15.63	58.88	29.9	0.0	70.1
AVE	50.81	0.74	12.25	35.96	48.49	1.68	16.09	33.25	57.9	2.2	39.9
SUM	99.76				99.51				100.0		

TABLE D.4   49A4-9 INCLUSION CHEMICAL COMPOSITIONS

SAMPLE: 49A4-9 TIG (Q: 60 kj/in)										
	Weight Percent (%)				Oxide Percent (%)				Oxide % w/o TiO2		
Incl	Al	Si	Ti	Mn	Al2O3	SiO2	TiO2	MnO	Al2O3	SiO2	MnO
1	55.10	0.00	7.04	37.67	54.08	0.00	8.42	38.45	58.4	0.0	41.6
2	55.41	1.47	6.55	37.50	54.54	1.01	6.33	38.45	58.0	1.1	40.9
3	73.87	0.22	3.11	23.53	75.57	0.51	5.25	18.70	79.7	0.5	19.7
4	57.18	0.00	4.10	38.76	62.38	0.00	5.00	32.84	65.5	0.0	34.5
5	57.87	0.00	4.84	37.88	55.25	0.00	6.90	37.92	59.3	0.0	40.7
6	58.17	1.23	18.47	21.64	41.31	3.55	22.53	32.67	53.3	4.6	42.1
7	18.58	0.52	18.78	63.00	35.44	0.16	25.23	40.22	46.7	0.2	53.0
8	57.05	1.38	4.34	35.84	54.14	0.77	10.73	35.32	60.0	0.9	39.1
9	57.80	1.57	15.12	25.66	54.00	0.45	12.55	33.00	61.7	0.5	37.7
10	54.26	0.00	7.85	37.80	52.33	0.00	9.43	37.95	58.0	0.0	42.0
11	54.42	0.00	4.88	40.88	58.39	0.00	4.72	37.92	60.6	0.0	39.4
12	78.85	0.00	4.54	16.84	80.34	0.00	4.47	15.26	84.0	0.0	16.0
13	48.38	0.56	9.35	41.71	49.89	0.45	13.93	36.05	57.7	0.5	41.7
14	53.50	0.75	11.12	34.22	49.73	1.71	14.88	33.71	58.4	2.0	39.6
15	55.35	0.00	6.18	38.43	70.73	0.00	5.10	24.17	74.5	0.0	25.5
16	64.02	0.00	2.32	33.80	55.19	0.00	7.72	37.02	59.9	0.0	40.1
17	75.53	0.00	4.88	19.72	77.00	0.00	4.71	18.34	80.8	0.0	19.2
18	72.70	0.00	4.05	23.35	77.30	0.00	4.45	18.88	80.4	0.0	19.6
19	78.21	0.00	4.39	17.63	85.61	0.00	4.20	10.25	89.3	0.0	10.7
20	81.78	0.00	4.18	14.10	84.65	0.00	4.34	11.04	88.5	0.0	11.5
AVE	60.40	0.39	7.30	32.00	61.39	0.43	9.04	29.41	66.7	0.5	32.7
SUM	100.09				100.27				99.9		

TABLE D.5   49B4-4 INCLUSION CHEMICAL COMPOSITIONS

	SAMPLE:			49B4-4	TIG	(Q: 100 kj/in)				
	Weight Percent (%)				Oxide Percent (%)			Oxide % w/o TiO2		
Incl	Al	Si	Ti	Mn	Al2O3	SiO2	TiO2	MnO	Al2O3	SiO2	MnO
1	50.97	0.00	16.56	32.46	46.16	0.00	22.32	31.51	59.4	0.0	40.6
2	50.13	0.00	14.36	35.51	47.48	0.00	20.08	32.44	59.4	0.0	40.6
3	52.66	0.00	11.99	35.34	49.81	0.00	16.23	33.97	59.5	0.0	40.5
4	33.45	2.31	18.72	45.53	40.13	5.92	26.52	27.43	54.6	8.1	37.3
5	59.16	0.00	11.80	29.04	56.91	0.00	14.71	28.38	66.7	0.0	33.3
6	23.92	1.85	20.09	54.15	38.68	4.71	26.80	29.81	52.8	6.4	40.8
7	23.92	1.65	20.09	54.15	47.07	0.00	20.82	32.11	59.4	0.0	40.6
8	8.99	3.94	59.99	27.11	15.26	8.44	51.93	24.38	31.7	17.6	50.7
9	48.31	0.34	15.82	34.94	44.70	2.23	22.52	30.55	57.7	2.9	39.4
10	62.17	0.00	11.70	26.13	61.03	0.00	14.20	24.77	71.1	0.0	28.9
11	46.14	3.38	12.98	37.50	42.90	8.26	19.52	29.32	53.3	10.3	36.4
12	43.59	2.35	15.31	38.75	42.00	5.99	23.30	28.70	54.8	7.8	37.4
13	64.77	0.00	13.09	22.13	64.04	0.00	15.43	20.53	75.7	0.0	24.3
14	18.68	1.13	57.20	22.98	31.82	2.83	44.97	20.38	57.8	5.1	37.0
15	48.46	0.00	19.30	32.24	43.52	0.00	26.75	29.73	59.4	0.0	40.6
16	19.85	0.53	25.99	53.63	33.60	1.31	33.50	31.59	50.5	2.0	47.5
17	48.64	0.20	16.25	22.82	45.45	0.47	23.02	31.05	59.0	0.6	40.3
18	57.67	0.00	15.28	34.91	53.78	0.00	19.02	27.21	66.4	0.0	33.6
19	46.62	0.53	16.43	36.42	44.24	1.33	24.20	30.23	58.4	1.8	39.9
20	49.57	1.58	17.02	31.83	43.51	3.56	23.21	29.72	56.7	4.6	38.7
AVE	42.88	0.99	20.50	35.38	44.61	2.25	24.45	28.69	58.2	3.4	38.4
SUM	99.75				100.00				100.0		

TABLE D.6   49C3-1 INCLUSION CHEMICAL COMPOSITIONS

| | SAMPLE: 49C3-1   TIG (Q: 60 kj/in) | | | | | | | | | |
| | Weight Percent (%) | | | | Oxide Percent (%) | | | | Oxide % w/o TiO2 | | |
Incl	Al	Si	Ti	Mn	Al2O3	SiO2	TiO2	MnO	Al2O3	SiO2	MnO
1	36.95	3.56	23.07	36.42	35.73	8.82	31.04	24.41	51.8	12.8	35.4
2	44.99	0.34	25.93	27.75	38.72	0.87	33.95	26.46	58.6	1.3	40.1
3	35.51	0.06	48.15	16.29	44.20	0.15	39.03	16.62	72.5	0.2	27.3
4	45.97	0.34	20.73	32.95	41.21	0.84	29.78	28.16	58.7	1.2	40.1
5	20.04	0.42	43.71	35.83	35.43	1.14	35.78	27.64	55.2	1.8	43.0
6	33.75	0.00	32.74	33.51	38.97	0.00	34.40	26.63	59.4	0.0	40.6
7	45.78	0.00	16.84	37.38	44.44	0.00	25.19	30.37	59.4	0.0	40.6
8	20.50	0.00	36.20	43.30	35.64	0.00	36.27	28.08	55.9	0.0	44.1
9	33.44	0.00	28.85	37.71	38.99	0.00	34.37	26.64	59.4	0.0	40.6
10	31.96	0.72	28.25	39.08	38.27	1.87	33.72	26.15	57.7	2.8	39.4
11	37.77	0.00	15.99	46.25	45.55	0.00	23.32	31.13	59.4	0.0	40.6
12	37.80	0.00	19.55	42.66	42.71	0.00	28.10	29.19	59.4	0.0	40.6
13	47.76	0.00	10.74	41.50	49.69	0.00	16.36	33.95	59.4	0.0	40.6
14	47.45	1.08	11.73	39.74	47.30	2.72	17.66	32.32	57.4	3.3	39.3
15	34.19	0.73	30.40	34.69	38.22	1.92	33.74	26.12	57.7	2.9	39.4
16	44.47	0.00	21.99	33.54	40.52	0.00	31.80	27.69	59.4	0.0	40.6
17	32.67	1.43	29.65	36.26	37.51	3.74	33.11	25.64	56.1	5.6	38.3
18	45.81	0.40	16.48	37.31	44.14	1.03	24.66	30.16	58.6	1.4	40.0
19	17.10	0.74	24.73	57.44	29.36	1.78	32.34	36.53	43.4	2.6	54.0
20	23.61	0.83	24.71	50.86	38.14	2.13	31.82	27.91	55.9	3.1	40.9
AVE	35.88	0.53	25.52	38.02	40.24	1.35	30.32	28.09	57.8	2.0	40.3
SUM	99.95				99.91				100.1		

60

TABLE D.7   50B3-2 INCLUSION CHEMICAL COMPOSITIONS

	SAMPLE:			50B3-2	TIG (Q: 50 kj/in)					
	Weight Percent (%)				Oxide Percent (%)				Oxide % w/o TiO2	
Incl	Al	Si	Ti	Mn	Al2O3	SiO2	TiO2	MnO	Al2O3	SiO2	MnO
1	28.91	0.16	16.30	54.63	45.39	0.43	22.36	31.81	58.5	0.6	41.0
2	36.62	12.35	8.86	42.17	34.30	28.41	13.84	23.44	39.8	33.0	27.2
3	46.12	0.38	10.36	43.13	49.24	1.02	16.09	33.65	58.7	1.2	40.1
4	32.55	4.19	16.35	46.92	39.24	10.54	23.40	26.82	51.2	13.8	35.0
5	37.38	6.11	12.85	43.67	38.95	15.06	19.36	26.62	48.3	18.7	33.0
6	18.35	20.12	12.96	48.38	27.40	33.87	18.28	20.45	33.5	41.4	25.0
7	27.09	18.45	11.89	42.57	29.18	33.02	17.86	19.94	35.5	40.2	24.3
8	23.41	4.75	10.53	61.31	36.69	10.98	14.23	38.10	42.8	12.8	44.4
9	23.20	25.05	10.66	41.09	29.73	33.66	16.29	20.32	35.5	40.2	24.3
10	15.54	12.89	20.35	51.22	23.09	27.86	26.44	22.62	31.4	37.9	30.7
11	7.00	13.18	16.15	63.67	11.22	26.02	21.34	41.42	14.3	33.1	52.7
12	36.65	4.52	12.06	46.77	41.94	11.43	17.96	28.67	51.1	13.9	34.9
13	23.28	12.86	14.14	49.72	30.53	28.67	19.64	21.16	38.0	35.7	26.3
14	33.52	0.28	11.70	54.49	49.05	0.74	16.58	33.62	58.8	0.9	40.3
15	28.62	12.60	15.69	43.09	29.34	28.11	22.50	20.05	37.9	36.3	25.8
16	39.31	2.16	11.90	46.63	45.44	5.63	17.87	31.06	55.3	6.9	37.8
17	36.03	0.00	12.07	51.89	49.01	0.00	17.49	33.50	59.4	0.0	40.6
18	15.36	9.07	20.27	55.30	24.10	20.21	26.86	28.83	33.0	27.6	39.4
19	23.69	13.48	13.50	49.33	30.38	29.77	18.91	20.94	37.5	36.7	25.8
20	7.62	10.82	10.42	71.14	12.11	20.76	13.64	53.49	14.0	24.0	61.9
AVE	27.01	9.17	13.45	50.36	33.82	18.31	19.05	28.83	41.7	22.7	35.5
SUM	99.99				100.01				99.9		

61

TABLE D.8   50B4-2 INCLUSION CHEMICAL COMPOSITIONS

Incl	Weight Percent (%)				Oxide Percent (%)				Oxide % w/o TiO2		
	Al	Si	Ti	Mn	Al2O3	SiO2	TiO2	MnO	Al2O3	SiO2	MnO
1	26.78	24.30	7.71	41.21	31.20	35.33	12.14	21.33	35.5	40.2	24.3
2	31.83	12.19	9.33	46.65	34.43	28.06	13.99	23.53	40.0	32.6	27.4
3	38.95	13.86	7.06	40.13	34.01	31.41	11.34	23.24	38.4	35.4	26.2
4	2.87	11.82	10.83	74.49	4.60	21.82	14.10	59.48	5.4	25.4	69.2
5	5.52	24.08	6.41	63.99	8.17	43.28	8.46	40.06	8.9	47.3	43.8
6	10.44	28.95	6.08	54.53	15.64	47.30	8.47	28.60	17.1	51.7	31.2
7	30.56	20.16	7.21	42.07	31.48	35.63	11.37	21.52	35.5	40.2	24.3
8	10.51	31.23	4.65	53.61	16.28	48.10	6.57	29.04	17.4	51.5	31.1
9	4.53	23.52	6.62	65.32	6.79	42.10	8.70	42.41	7.4	46.1	46.5
10	5.84	24.96	9.50	59.69	8.59	45.27	12.69	33.45	9.8	51.8	38.3
11	44.06	2.01	7.84	46.09	49.02	5.29	12.20	33.50	55.8	6.0	38.2
12	14.64	27.13	4.83	53.34	21.52	44.62	6.91	26.95	23.1	47.9	29.0
13	23.45	21.05	7.23	48.20	31.51	36.01	10.73	21.75	35.3	40.3	24.4
14	41.18	6.98	7.38	44.76	42.28	17.26	11.57	28.89	47.8	19.5	32.7
15	33.55	9.54	7.36	49.55	39.41	22.71	10.95	26.94	44.3	25.5	30.2
16	8.28	27.04	3.51	61.17	11.68	48.41	4.70	35.22	12.3	50.8	37.0
17	13.47	35.26	4.63	46.64	24.44	42.76	7.00	25.61	26.3	46.1	27.6
18	21.10	14.63	10.24	54.04	29.50	31.56	14.12	24.83	34.3	36.7	28.9
19	37.86	8.77	10.26	43.12	37.52	21.04	15.81	25.64	44.6	25.0	30.5
20	26.38	13.84	10.13	49.65	32.42	30.61	14.55	22.22	38.0	35.9	26.1
AVE	21.59	19.07	7.44	51.91	25.53	33.93	10.82	29.71	28.9	37.8	33.3
SUM	100.01				99.99				100.0		

SAMPLE: 50B4-2 TIG (Q: 100 kj/in)

TABLE D.9 51B4-6 INCLUSION CHEMICAL COMPOSITIONS

	SAMPLE:			51B4-6	TIG (Q: 100 kj/in)					
	Weight Percent (%)				Oxide Percent (%)				Oxide % w/o TiO2		
Incl	Al	Si	Ti	Mn	Al2O3	SiO2	TiO2	MnO	Al2O3	SiO2	MnO
1	19.19	9.06	13.70	62.05	30.72	11.43	18.38	39.47	37.6	14.0	48.4
2	9.47	10.36	9.83	69.75	14.91	21.29	12.83	50.91	17.1	24.4	58.4
3	16.60	6.45	10.28	66.67	26.31	13.60	13.65	46.44	30.5	15.7	53.8
4	22.83	17.28	10.06	49.81	30.19	34.34	14.34	21.13	35.2	40.1	24.7
5	43.30	0.38	3.58	46.13	55.51	1.0	5.55	37.34	59.1	1.1	39.8
6	6.97	11.56	11.12	70.36	11.08	22.14	14.56	52.22	13.0	25.9	61.1
7	14.03	17.34	6.63	60.00	20.39	34.41	11.56	33.62	23.1	38.9	38.0
8	7.24	12.74	6.87	73.15	11.27	23.76	6.93	56.04	12.4	26.1	61.5
9	24.61	7.63	11.76	55.81	36.93	18.00	16.12	28.35	44.3	21.6	34.0
10	17.29	8.07	10.35	63.68	26.33	17.25	14.61	41.15	31.1	20.4	48.6
11	8.04	10.54	3.41	78.01	12.41	19.32	4.40	63.87	13.0	20.2	66.8
12	7.96	2.33	15.24	74.47	13.33	4.66	20.16	61.85	16.7	5.8	77.5
13	8.85	17.23	9.64	64.09	13.43	32.92	12.99	40.65	15.4	37.8	46.7
14	11.04	9.66	10.44	68.86	17.46	19.17	13.73	49.64	20.2	22.2	57.5
15	28.81	10.56	9.93	50.71	36.25	24.65	14.28	24.82	42.3	28.8	29.0
16	16.87	9.16	12.64	61.33	26.16	19.74	16.93	37.17	31.5	23.8	44.7
17	1.63	1.23	18.53	78.61	2.77	2.36	24.62	70.25	3.7	3.1	93.2
18	25.66	0.86	9.01	64.47	41.44	2.02	12.15	44.39	47.2	2.3	50.5
19	26.36	3.53	11.61	56.50	41.32	8.62	15.84	34.22	49.1	10.2	40.7
20	35.07	1.26	7.68	55.99	50.89	3.27	10.91	34.94	57.1	3.7	39.2
AVE	17.59	8.66	9.84	63.52	23.96	16.70	13.73	43.42	30.0	19.3	50.7
SUM	99.61				97.81				100.0		

TABLE D.10   51C2-3 INCLUSION CHEMICAL COMPOSITIONS

	SAMPLE:		51C2-3 TIG (Q: 100 kj/in)							
	Weight Percent (%)				Oxide Percent (%)				Oxide % w/o TiO2		
Incl	Al	Si	Ti	Mn	Al2O3	SiO2	TiO2	MnO	Al2O3	SiO2	MnO
1	15.39	24.14	14.09	46.38							
2	5.89	18.47	10.91	64.73	9.07	34.55	14.36	42.02	10.6	40.3	49.1
3	30.83	10.34	9.23	49.00	36.17	25.53	13.58	24.72	41.9	29.5	28.6
4	29.87	9.73	14.29	46.11	33.56	22.81	20.70	22.93	42.3	28.8	28.9
5	19.91	9.03	12.01	58.38	30.28	20.19	16.23	33.00	36.3	24.2	39.5
6	19.66	33.47	5.68	41.20	32.27	36.65	8.95	22.12	35.4	40.3	24.3
7	21.89	12.74	12.63	52.74	30.78	28.34	17.40	23.49	37.3	34.3	28.4
8	29.58	4.63	13.25	52.54	41.36	11.62	18.63	28.39	50.8	14.3	34.9
9	14.11	12.13	14.04	59.73	21.63	25.42	18.78	34.18	26.6	31.3	42.1
10	6.83	18.14	12.36	62.67	10.49	34.48	16.35	38.68	12.5	41.2	46.2
11	22.08	10.63	15.64	51.65	31.40	24.34	21.31	22.99	39.9	30.9	29.2
12	26.23	15.31	13.33	45.13	29.01	31.85	19.31	19.83	36.0	39.5	24.6
13	15.17	22.34	13.02	49.47	23.37	36.39	18.28	21.97	28.6	44.5	26.9
14	8.82	21.16	13.36	56.06	12.98	40.34	18.76	27.92	16.0	49.7	34.4
15	25.97	15.50	11.97	46.56	29.77	32.50	17.38	20.35	36.0	39.3	24.6
16	19.65	11.76	11.88	56.71	28.92	25.75	16.51	29.18	34.5	30.7	34.8
17	20.62	11.81	12.68	54.90	29.98	26.24	17.32	26.45	36.3	31.7	32.0
18	4.52	7.75	16.00	71.73	7.50	15.08	21.05	56.37	9.5	19.1	71.4
19	17.12	21.78	12.93	48.17	26.31	34.55	18.29	20.86	32.2	42.3	25.5
20	12.98	22.95	11.98	52.09	19.41	39.84	16.62	24.12	23.3	47.8	28.9
AVE	18.36	15.69	12.56	53.29	25.49	28.76	17.36	28.40	30.8	34.7	34.4
SUM	99.90				100.01				99.9		

64

TABLE D.11   75C3-10 INCLUSION CHEMICAL COMPOSITIONS

SAMPLE: 75C3-10 TIG (Q: 100 kj/in)										
Weight Percent (%)				Oxide Percent (%)				Oxide % w/o TiO2		
Incl	Al	Si	Ti	M n	Al2O3	SiO2	TiO2	MnO	Al2O3	SiO2	MnO
1	8.54	21.01	10.35	59.49	12.61	39.78	14.63	32.98	14.8	46.6	38.6
2	12.43	31.72	5.06	50.72	20.42	45.04	7.35	27.19	22.0	48.6	29.3
3	6.59	23.60	4.66	65.15	9.68	42.48	6.13	41.70	10.3	45.3	44.4
4	9.14	27.31	3.92	59.63	12.80	48.95	5.27	32.98	13.5	51.7	34.8
5	7.16	23.12	4.38	65.34	10.50	41.79	5.77	41.94	11.1	44.3	44.5
6	12.87	38.06	3.41	45.66	24.41	43.88	5.23	26.48	25.8	46.3	27.9
7	4.74	1.54	18.92	74.80	8.12	3.07	25.13	63.68	10.8	4.1	85.1
8	11.72	24.06	7.51	56.71	16.49	44.33	10.22	28.72	18.4	49.5	32.1
9	14.36	24.92	7.40	53.31	20.93	42.80	10.36	25.91	23.3	47.7	28.9
10	9.34	25.69	10.39	54.52	13.87	44.88	14.26	27.22	16.1	52.2	31.7
11	17.13	15.91	16.80	50.16	24.57	32.36	22.50	20.58	31.7	41.7	26.6
12	15.39	18.08	14.44	52.03	22.13	35.69	19.69	22.49	27.6	44.4	28.0
13	17.16	25.36	7.64	49.85	26.37	39.04	11.02	23.56	29.6	43.9	26.5
14	10.42	18.67	9.49	61.41	15.43	35.94	12.64	35.99	17.7	41.1	41.2
15	9.21	23.28	4.98	62.53	13.26	42.79	6.62	37.34	14.2	45.8	40.0
16	5.44	20.09	5.07	69.41	8.22	36.25	6.59	48.95	8.8	38.8	52.4
17	14.01	0.92	20.81	64.28	24.18	2.10	27.73	45.99	33.5	2.9	63.6
18	33.49	5.16	12.85	48.56	40.69	12.78	18.72	27.81	50.1	15.7	34.2
19	40.53	2.10	14.09	43.28	43.57	5.43	21.21	29.77	55.3	6.9	37.8
20	39.96	6.28	14.38	45.36	46.25	0.76	21.39	31.61	58.8	1.0	40.2
AVE	14.98	18.84	9.83	56.61	20.73	32.01	13.62	33.64	24.7	35.9	39.4
SUM	100.26				100.00				100.0		

TABLE D.12   75C4-11 INCLUSION CHEMICAL COMPOSITIONS

	SAMPLE:		75C4-11	TIG (Q: 50 kj/in)						
	Weight Percent (%)				Oxide Percent (%)				Oxide % w/o TiO2		
Incl	Al	Si	Ti	M n	Al2O3	SiO2	TiO2	MnO	Al2O3	SiO2	MnO
1	2.48	5.79	19.64	72.09	4.23	11.35	25.97	58.45	5.7	15.3	79.0
2	10.91	6.50	17.63	64.96	18.05	13.72	23.39	44.84	23.6	17.9	58.5
3	18.65	6.10	21.75	53.50	29.54	14.37	28.58	27.51	41.4	20.1	38.5
4	17.48	2.00	21.89	58.64	29.52	4.76	29.01	36.71	41.6	6.7	51.7
5	4.56	1.84	20.28	73.33	7.87	3.70	26.95	61.48	10.7	5.1	84.2
6	22.09	8.39	15.25	54.27	33.08	19.62	20.73	26.57	41.7	24.8	33.5
7	5.50	3.37	14.54	76.58	9.14	6.54	19.17	65.15	11.3	8.1	80.6
8	10.12	21.35	11.89	56.63	14.66	40.80	16.04	28.50	17.5	48.6	33.9
9	7.99	23.29	12.14	56.57	11.70	43.20	16.36	28.75	14.0	51.6	34.4
10	20.38	2.60	20.60	56.42	33.60	6.37	27.42	32.61	46.3	8.8	44.9
11	9.78	21.96	7.16	61.09	14.15	41.11	9.55	35.18	15.6	45.5	38.9
12	9.48	12.14	10.36	68.02	14.86	23.66	13.61	47.87	17.2	27.4	55.4
13	25.84	12.54	9.63	51.99	34.24	28.32	13.58	23.86	39.6	32.8	27.6
14	12.90	13.09	11.91	62.11	19.74	26.60	15.85	37.82	23.5	31.6	44.9
15	10.00	21.05	11.56	57.39	14.53	40.30	15.56	29.60	17.2	47.7	35.1
16	14.59	8.35	15.86	61.20	23.23	18.05	21.16	37.55	29.5	22.9	47.6
17	21.18	5.89	16.95	55.98	33.21	14.01	22.86	29.92	43.1	18.2	38.8
18	10.20	11.17	20.01	58.62	16.33	23.39	26.48	33.8	22.2	31.8	46.0
19	9.32	17.65	13.23	59.80	14.07	34.47	17.63	33.82	17.1	41.9	41.1
20	16.96	16.27	13.72	53.04	24.13	33.83	18.72	23.33	29.7	41.6	28.7
AVE	13.02	11.07	15.30	60.61	19.99	22.41	20.43	37.17	25.4	27.4	47.2
SUM	100.00				100.00				100.0		

66

APENDIX E

INCLUSION MnO-SiO2-Al2O3 PHASE DIAGRAM PLOTS
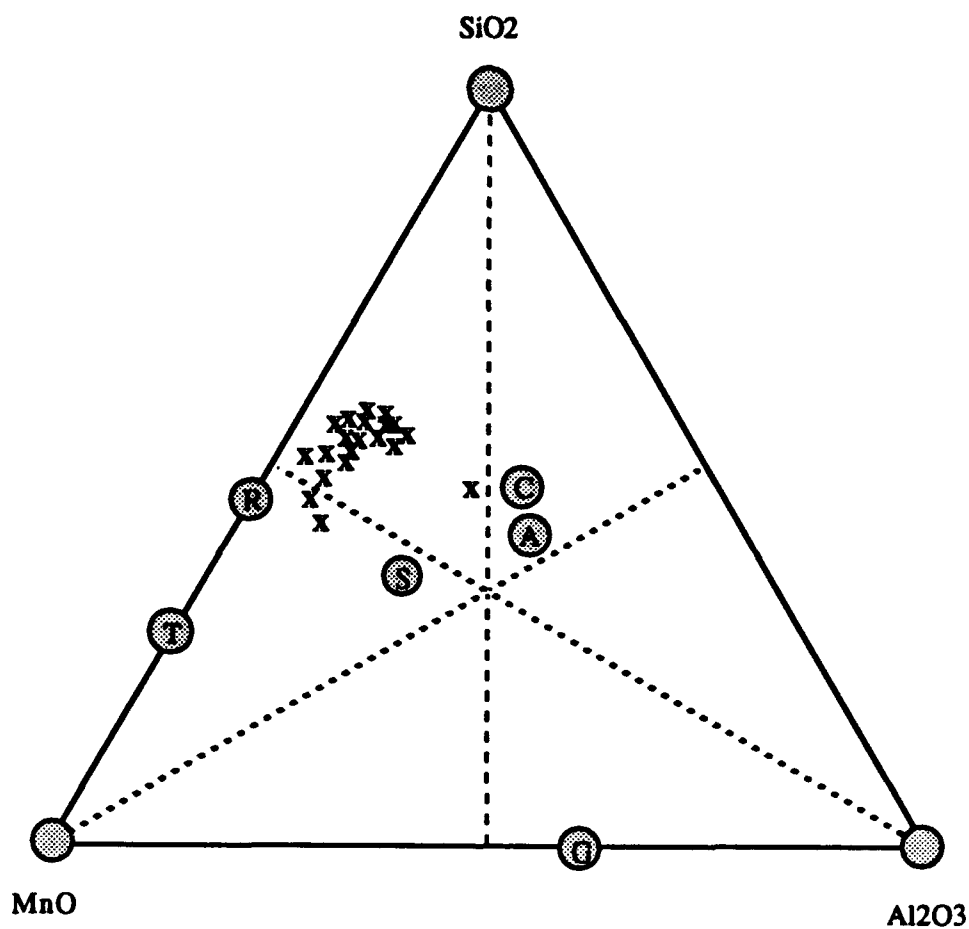
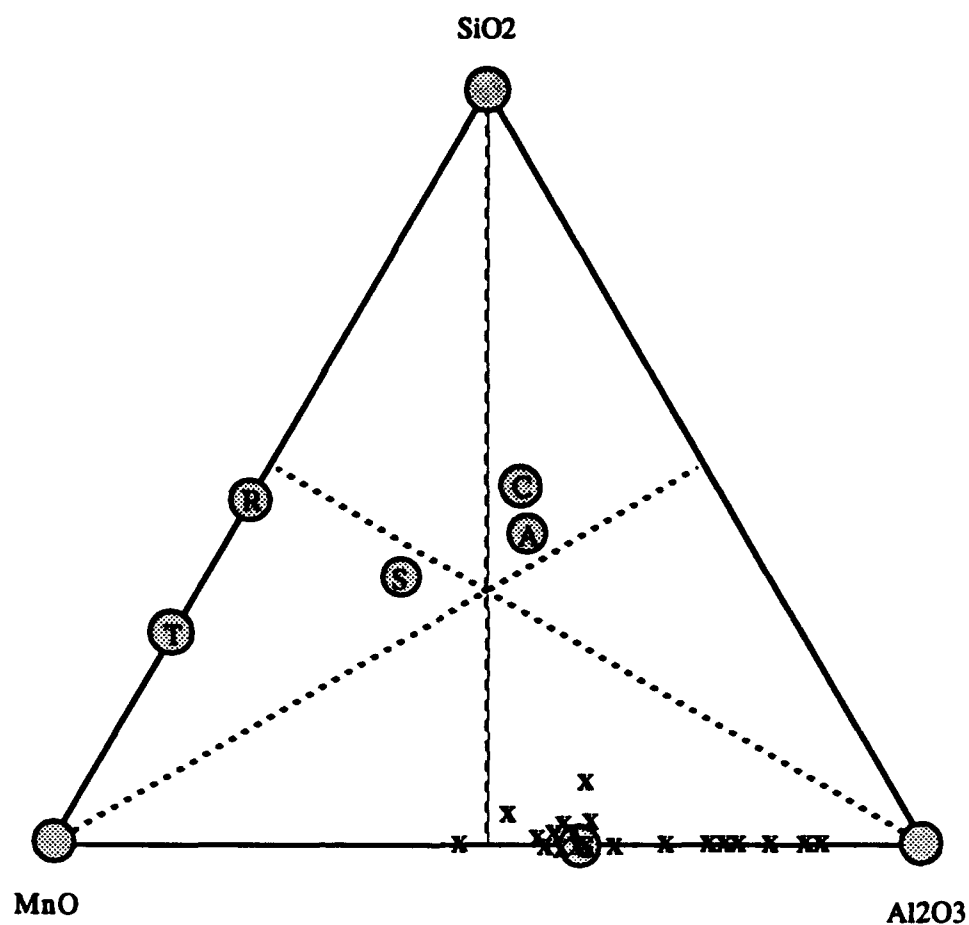**Figure E.1   32A3-G3 Inclusion Composition Plot**
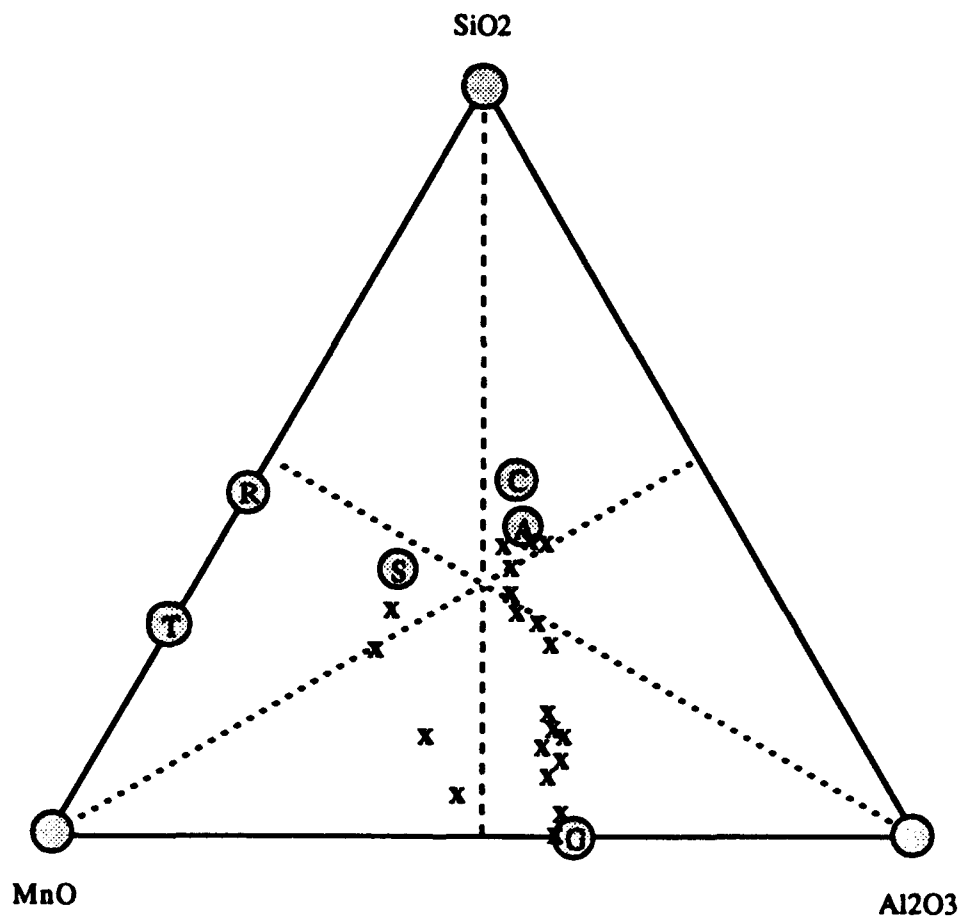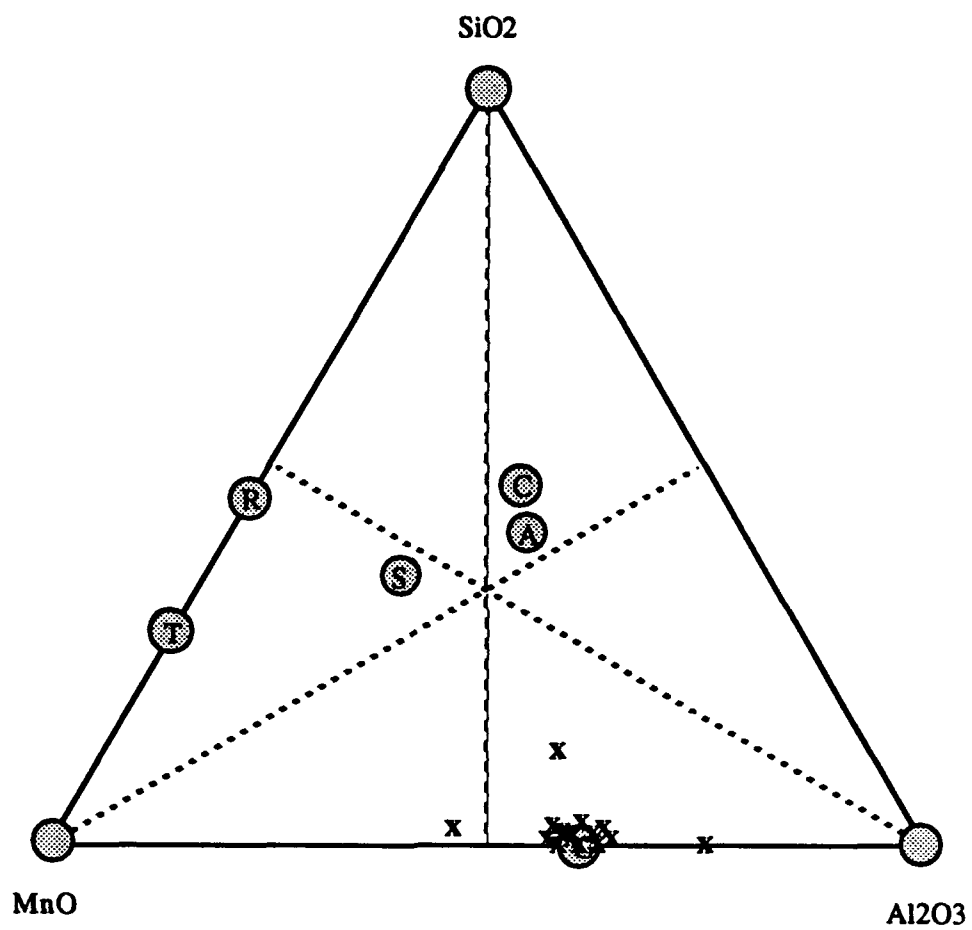
Figure E.2   29B4-10 Inclusion Composition Plot
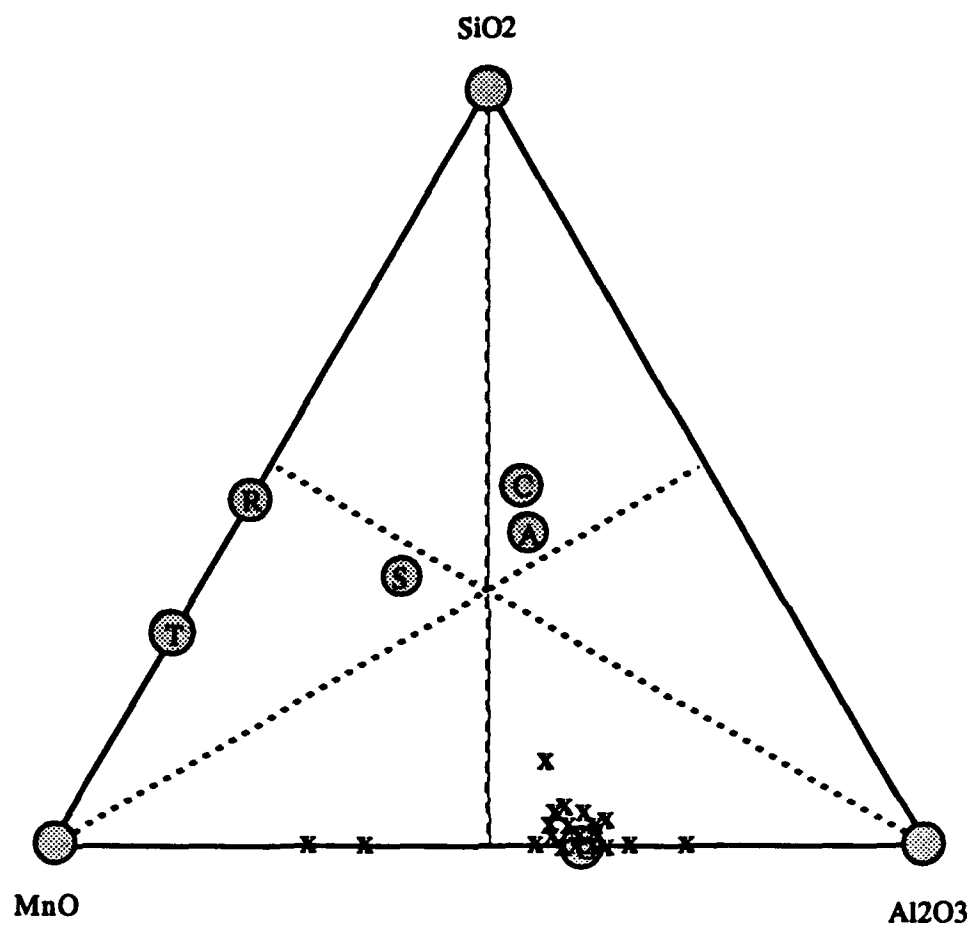
Figure E.3   49A3-11 Inclusion Composition Plot
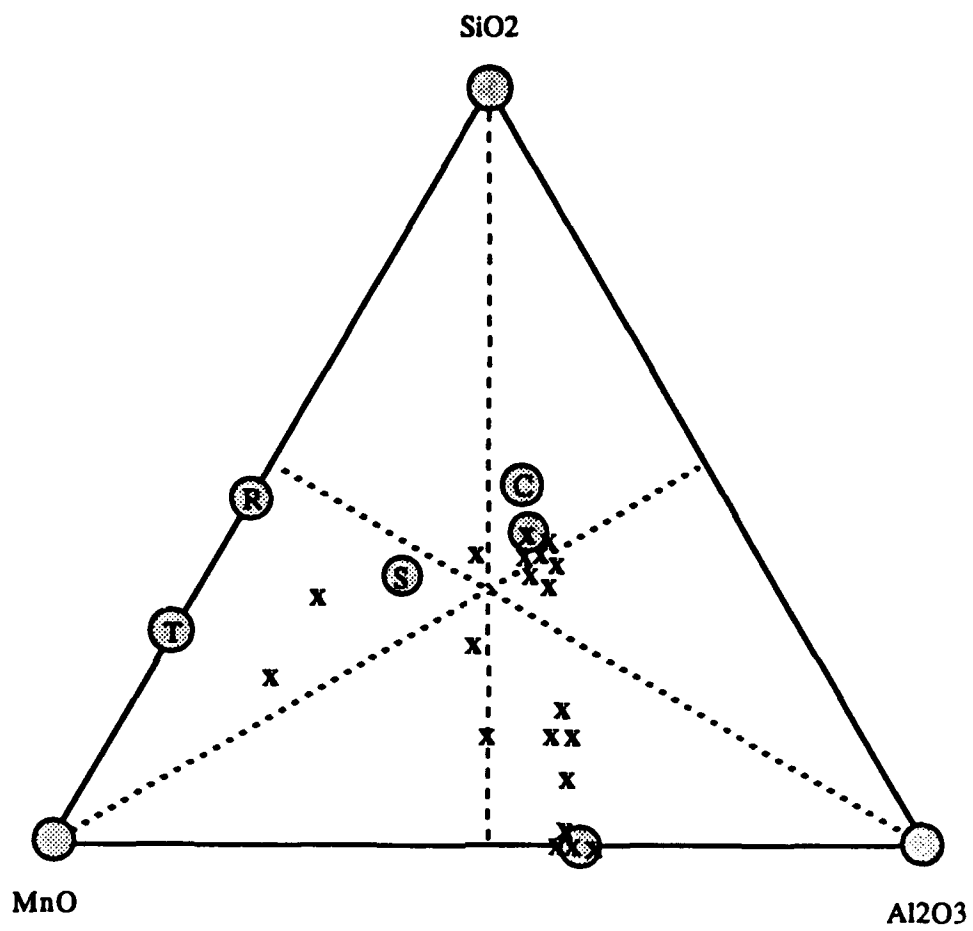
Figure E.4   49A4-9 Inclusion Composition Plot

70

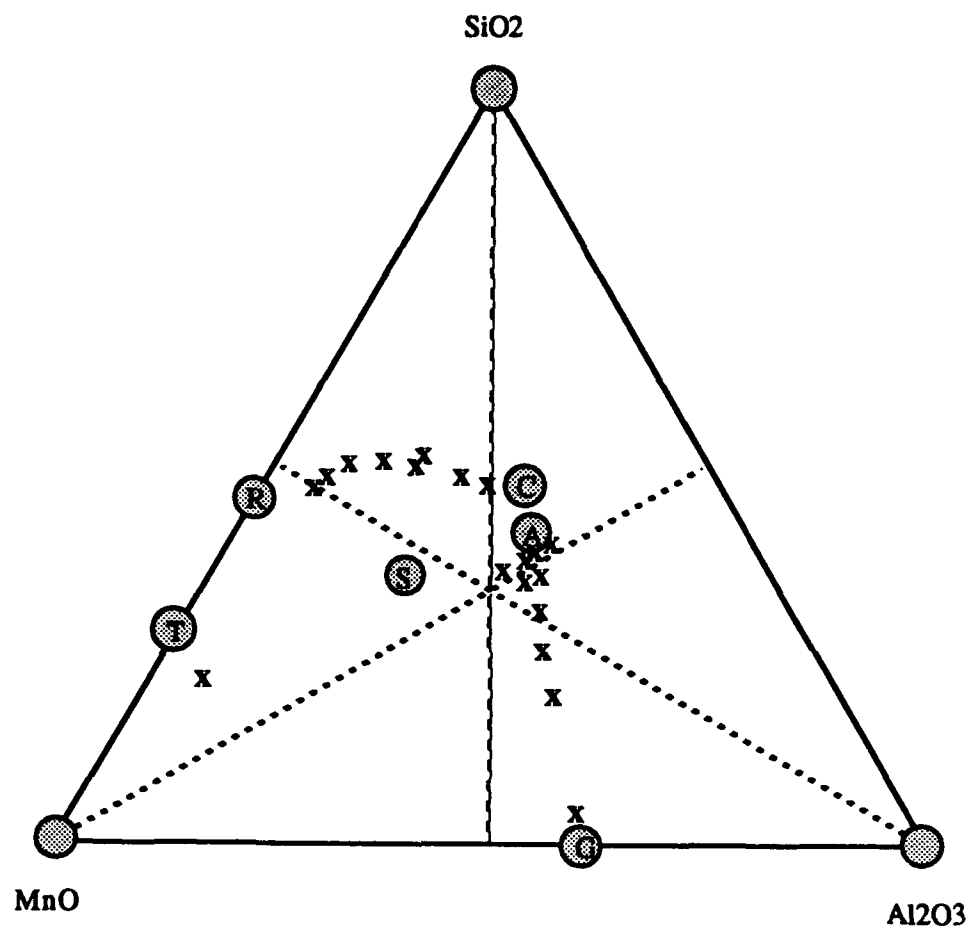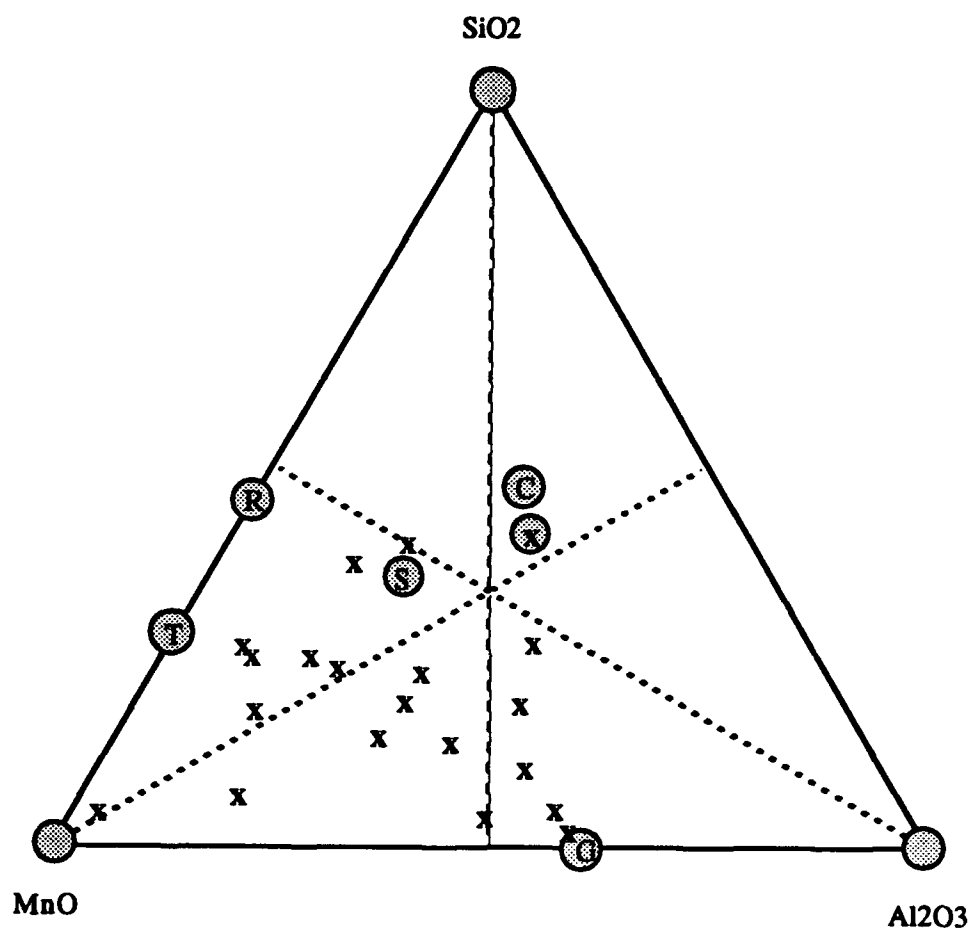**Figure E.5   49B4-4 Inclusion Composition Plot**
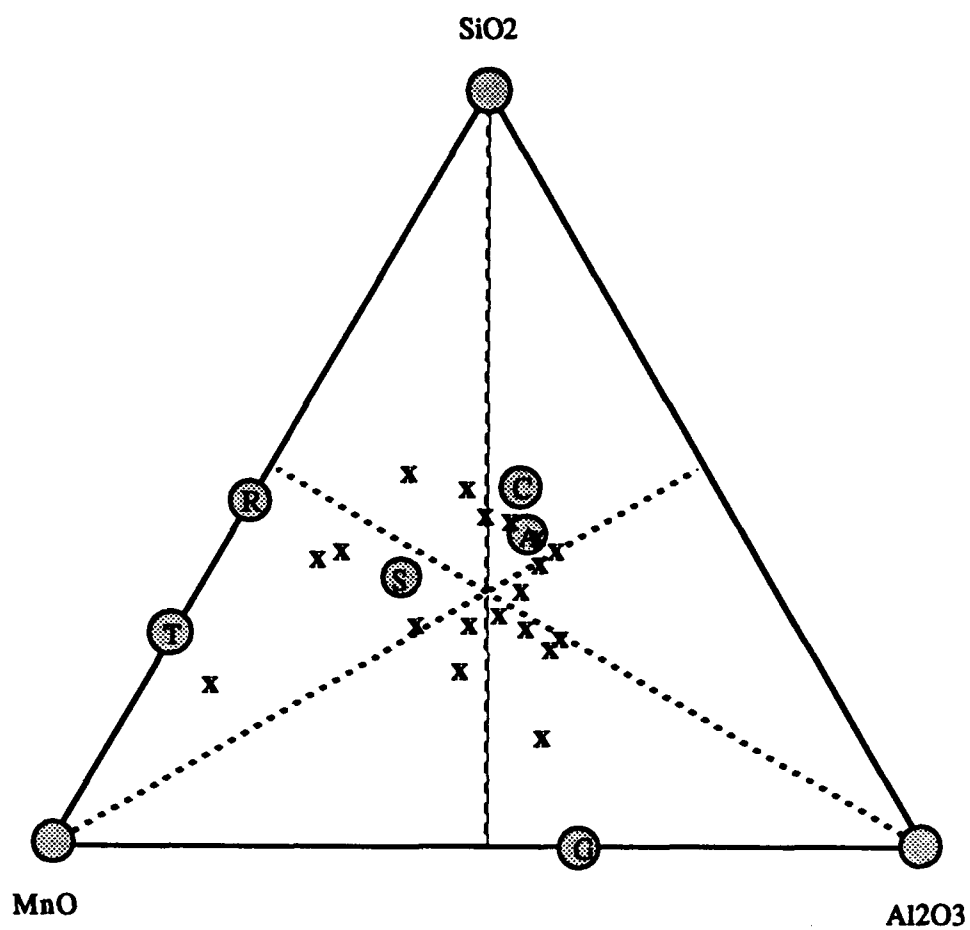
Figure E.6   49C3-1 Inclusion Composition Plot
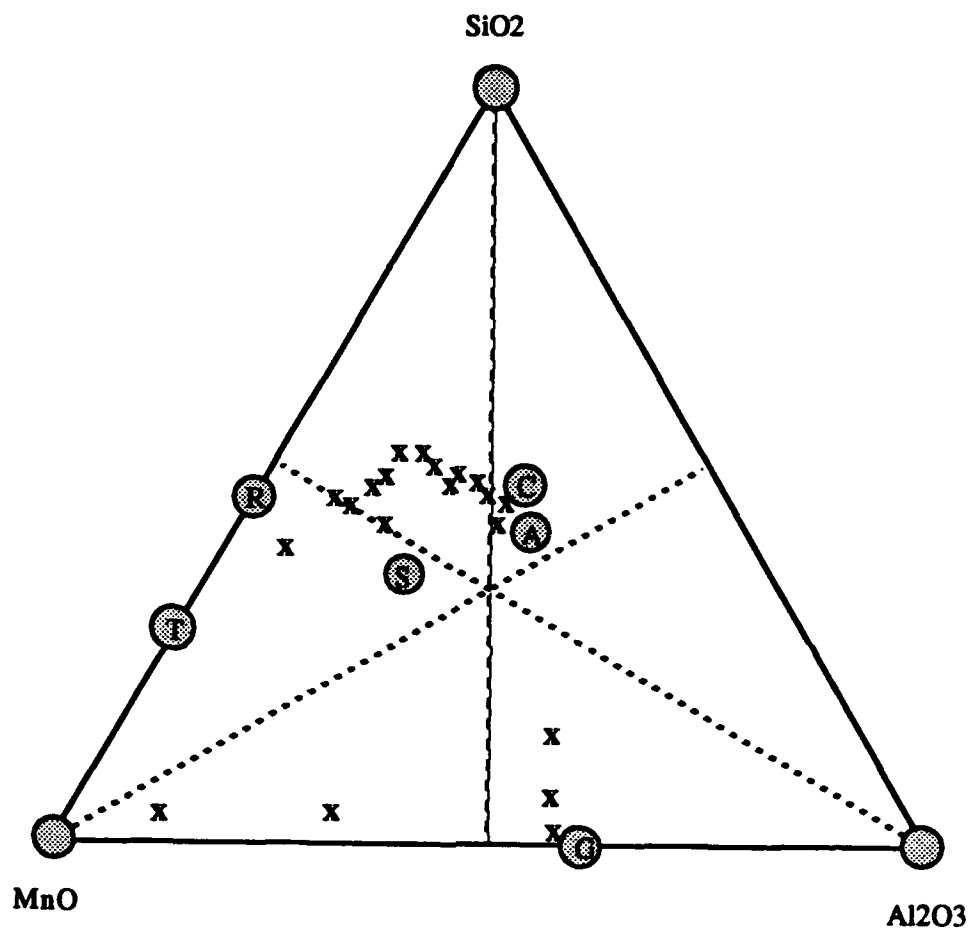
Figure E.7   50B3-2 Inclusion Composition Plot
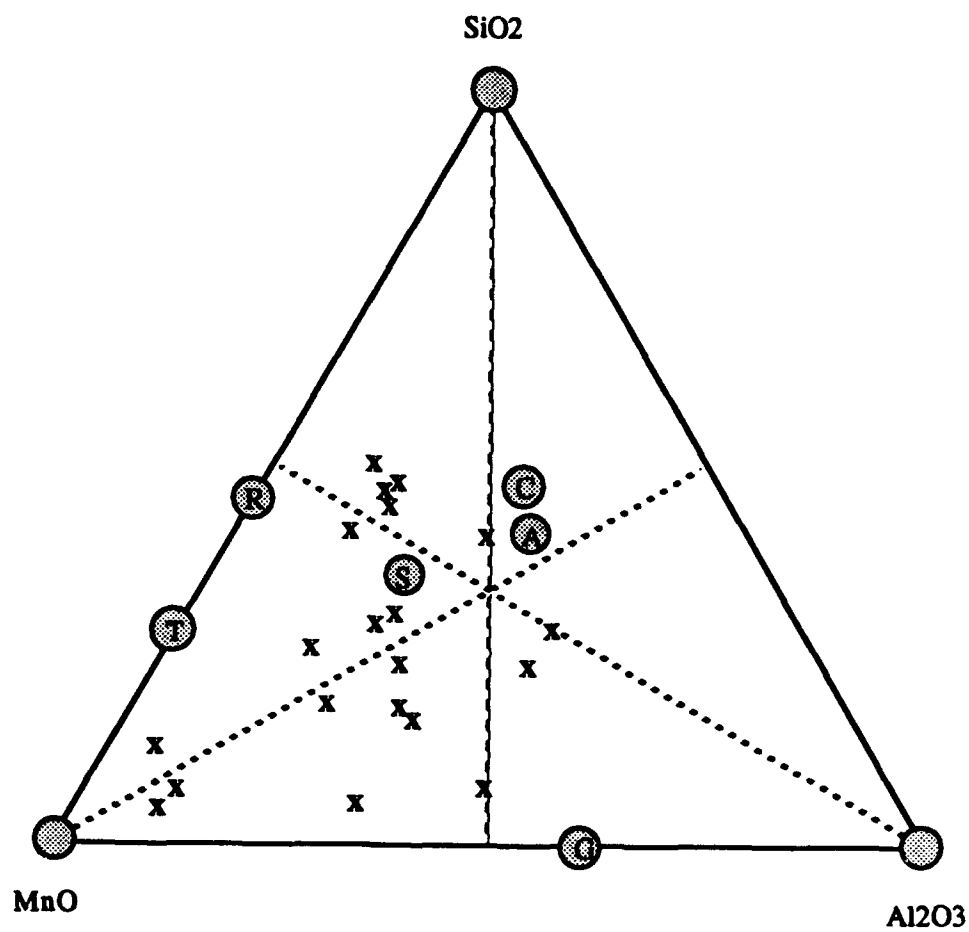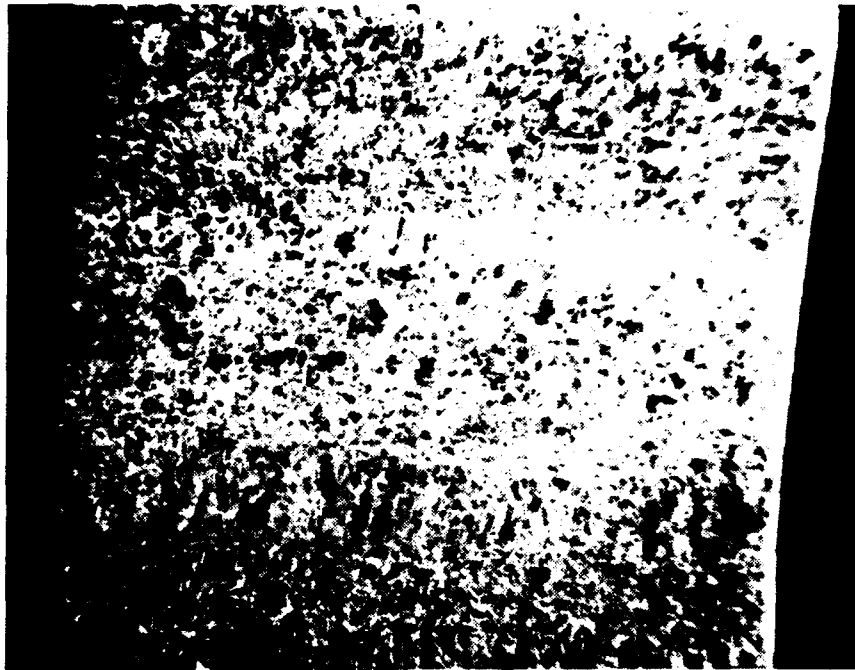
Figure E.8   50B4-2 Inclusion Composition Plot

74

Figure E.9   51B4-6 Inclusion Composition Plot

Figure E.10   51C2-3 Inclusion Composition Plot

Figure E.11   75C3-10 Inclusion Composition Plot

Figure E.12   75C4-11 Inclusion Composition Plot

APPENDIX F - OPTICAL MICROGRAPHS

Figure F.1   **29B4-10 Optical Micrograph (30X)**

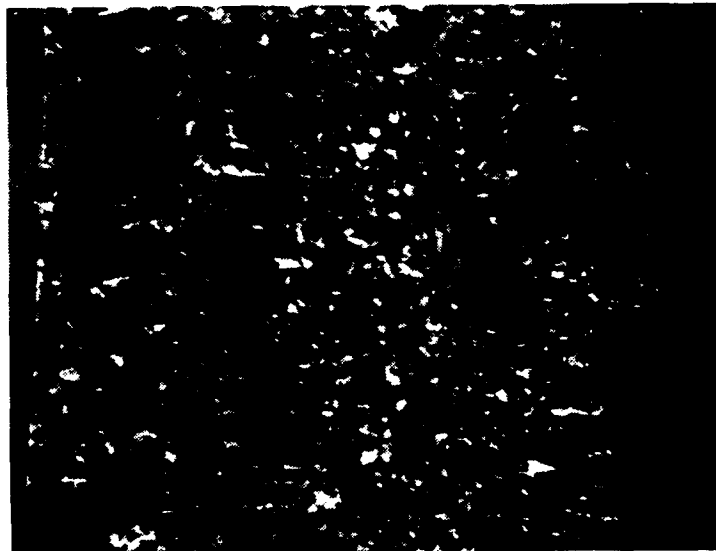**NOTE:** All Micrographs in Appendix F were taken with the sample face containing the Charpy V-Notch located at the bottom of the figure
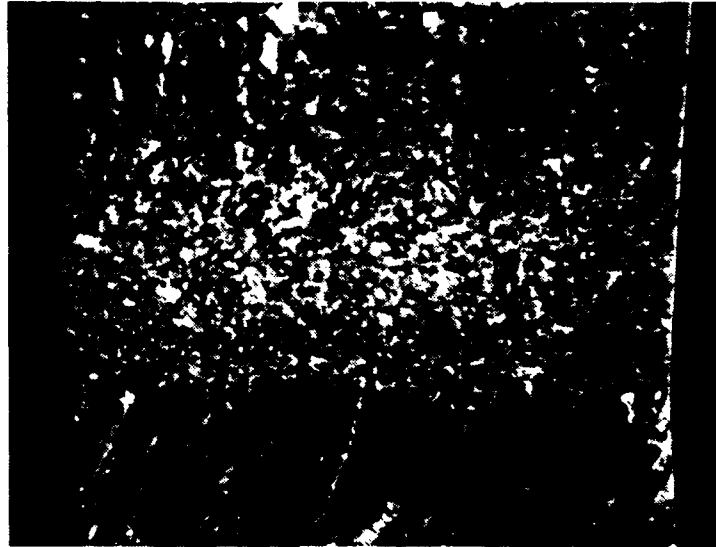
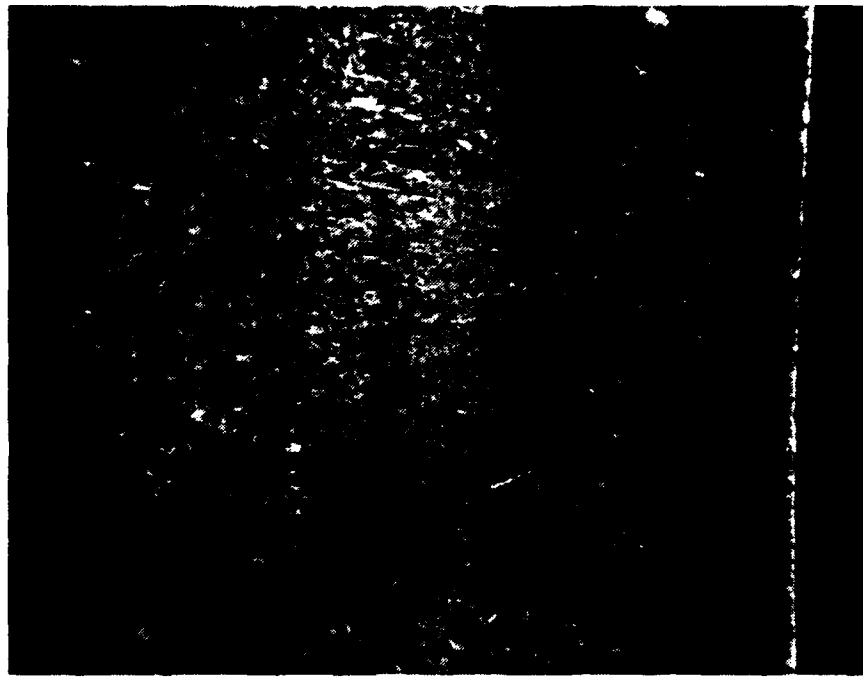**Figure F.2   49A3-11 Optical Micrograph (25X)**

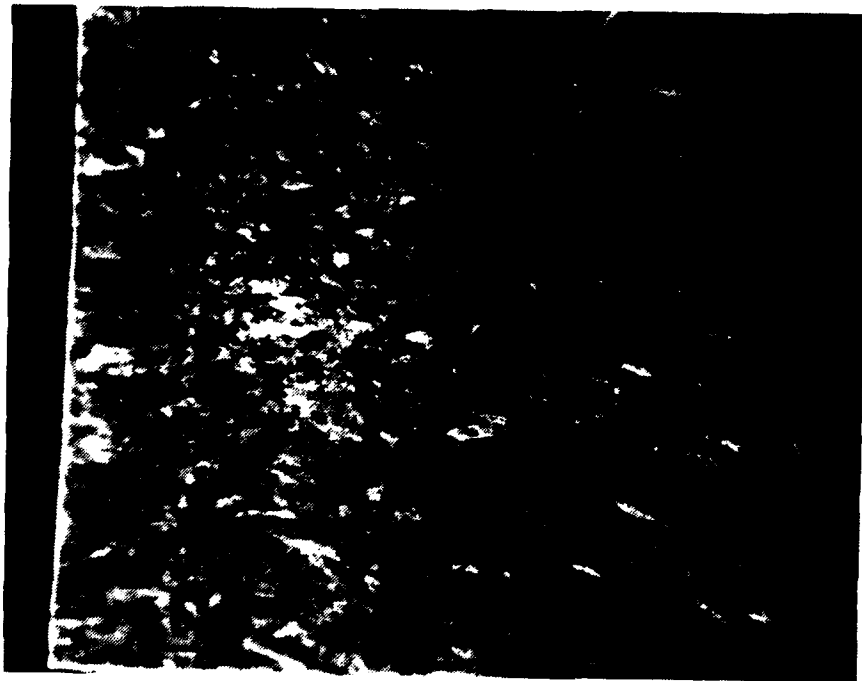**Figure F.3   49A4-9 Optical Micrograph (25X)**
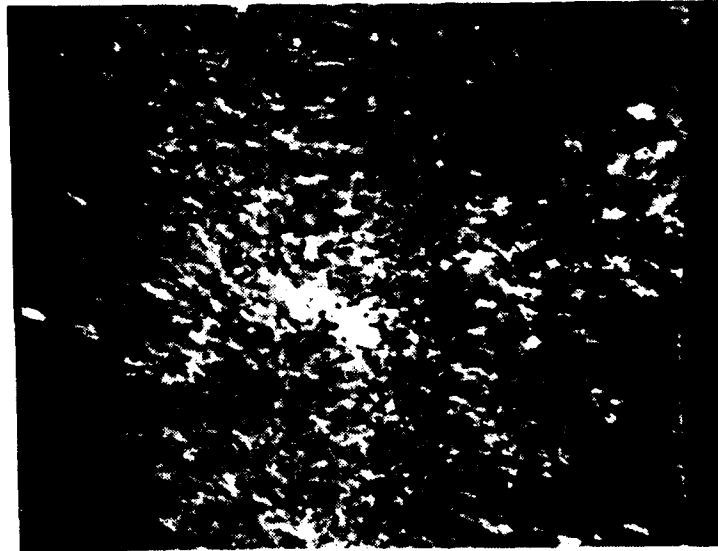
Figure F.4   49B4-4 Optical Micrograph (25X)

Figure F.5   49C3-1 Optical Micrograph (25X)

81

Figure F.6   **50B3-2 Optical Micrograph (30X)**
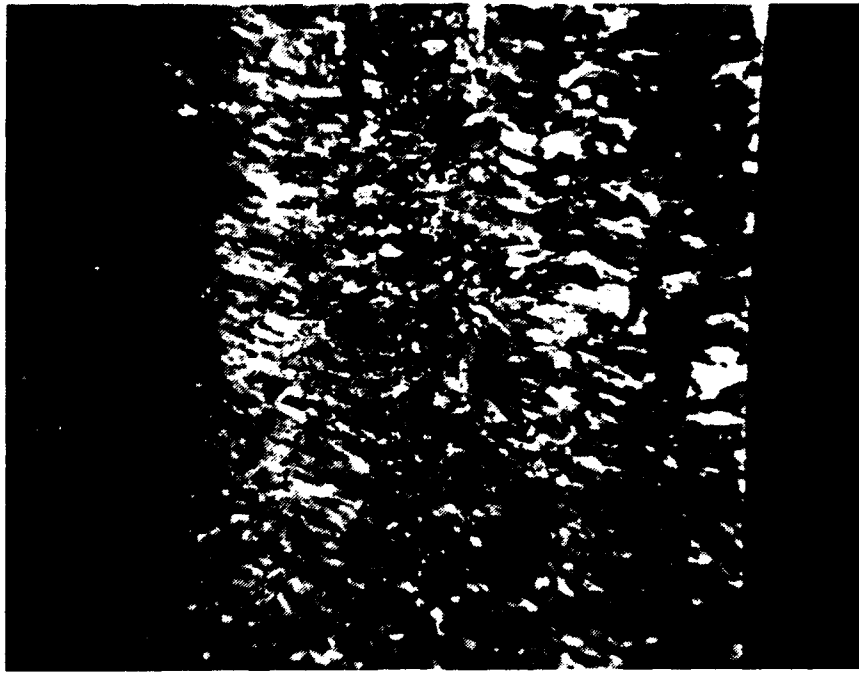

Figure F.7   **50B4-2 Optical Micrograph (30X)**
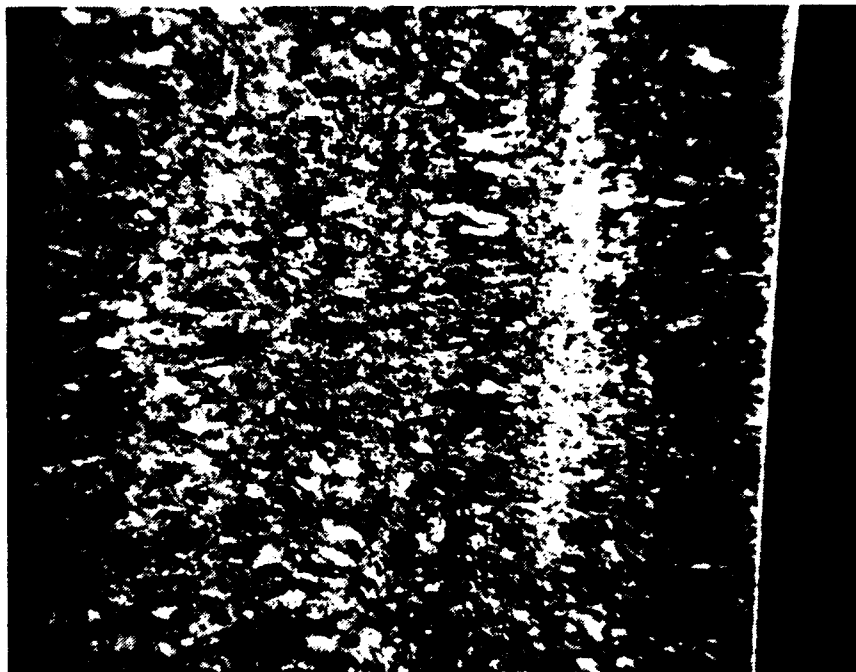
82

Figure F.8   51B4-6 Optical Micrograph (30X)

Figure F.9   51C2-3 Optical Micrograph (30X)

Figure F.10 **75C3-10 Optical Micrograph (30X)**

Figure F.11 **75C4-11 Optical Micrograph (30X)**

84

Figure F.12   32A3-G3 MIG Optical Micrograph (20X)

LIST OF REFERENCES

ASM International, *Binary Alloy Phase Diagrams*, 2d ed.,ASM International, 1990.

Blicharski, M.R., and others, "Structure and Properties of ULCB Plate Steels for Heavy Section Applications", *Processing, Microstructure and Properties of HSLA Steels*, The Minerals, Metals, and Materials Society, 1988.

Callister, W.D., *Materials Science And Engineering*, 2d ed., John Wiley and Sons, Inc., 1991.

Kiessling, R. and Lange, N., *Non-metallic Inclusions In Steel*, The Metals Society, London, 1987.

Kou, S., *Welding Metallurgy*, John Wiley and Sons, Inc., 1987.

Lancaster, J.F., *The Metallurgy of Welding, Brazing and Soldering*, George Allen and Unwin Ltd, 1965.

McDonald, E.P., Factors Influencing the Microstructure and Mechanical Properties of Ultra Low Carbon Bainitic 100 Tungsten Inert Gas Multipass Weldments, Master's Thesis, Naval Postgraduate School, Monterey, California, September, 1992.

Naval Surface Warfare Center Report CRDKNSWC-SSM-61-93/12, *The Effects of Alloying Elements on the Strength and Cooling Rate Sensitivity of Ultra-Low-Carbon Alloy Steel Weld Metals*, by M.G. Vassilaros, 1993.

Pickering, F.B., *Physical Metallurgy and the Design of Steels*, Applied Science Publishers, 1978.

Stinchcomp, C., *Welding Technology Today*, Prentice-Hall, Inc., 1989.

INITIAL DISTRIBUTION LIST

1. Defense Technical Information Center   2
    Cameron Station
    Alexandria, VA.   22304-6145

2. Superintendent   2
    Library, Code 52
    Naval Postgraduate School
    Monterey, CA.   93943-5002

3. Department Chairman, Code ME/Kk   1
    Department of Mechanical Engineering
    Naval Postgraduate School
    Monterey, CA.   93943-5000

4. Weapons Engineering Curricular Office, Code 33   1
    Naval Postgraduate School
    Monterey, CA.   93943-5000

5. Professor A.G. Fox, Code ME/Fx   2
    Department of Mechanical Engineering
    Naval Postgraduate School
    Monterey, CA.   93943-5000

6. Dr. M.G. Vassilaros, Code 2814   1
    Naval Surface Warfare Center
    Annapolis, MD.   21402

7. Lt Daniel E. Butler, USN   3
    5721 North 27 Road
    Arlington, VA.   22207